



A new preliminary system design of using geothermal well brine heater for desalination/nanofiltration process

Abdullah Almtairi^a, Mohamed A. Sharaf Eldean^{b,*}, A.M. Soliman^{b,c}, Abdelnasser Mabrouk^d, Hassan E.S. Fath^e

^a Civil & Environmental Engineering Department, Faculty of Science & Engineering, University of Wolverhampton, UK

^b Department of Mechanical Engineering, Faculty of Engineering, Suez University, Egypt

^c Mechanical Engineering Department, Faculty of Engineering, Jouf University, Sakaka, Saudi Arabia

^d Qatar Environment and Energy Research Institute, Hamad Bin Khalifa University, Qatar Foundation, Doha, Qatar

^e Desalination and Energy Systems (DES), Calgary, AB, Canada

ARTICLE INFO

Keywords:

Geothermal well
Nanofiltration
Desalination
Direct vapor generation
Brine heater
Condensation

ABSTRACT

In this work, a novel system design of using geothermal well energy acting as a brine heater for desalination purposes has been numerically developed and investigated. The system contains a pumping unit, nanofiltration, flash evaporation unit, and end condenser for condensation and freshwater production. The system aimed to pump the pre-treatment brine flow into the geothermal well (abandoned oil well) benefiting from its energy considering the well as an underground brine heater. It is anticipated by the geothermal well to increase the brine temperature up to an optimized value (40–50 °C). A Flash evaporation tank has been used as a steam generator. The brine blowdown will be dumped into the sea. To prevent corrosion and tubes deterioration, the Nanofiltration system has been used as a pre-stage before pumping the saline flow into the geothermal well. Reducing the salinity gradient was considered an important issue during this study. The salt-free steam will be directly flowing towards the condenser unit for condensation and freshwater production. It is expected to produce an amount of freshwater in the range of 500 to 1500m³/day. Results reveal that the total hourly costs are 1.185\$/h and total water price was in the range of 0.12\$/m³ to 1.2\$/m³ depending on the performance and salinity concentration of the Nanofiltration system.

1. Introduction

Water and its natural resources are considered an especially important part of living on the earth. Water is important for the proceeding of all life needs and in all life fields like agriculture's needs, human needs, and artificial needs. However, in the last few decades, water shortage problems appeared in many countries especially developing countries. Many remote areas of the world such as coastal desert areas in the Middle East or some Mediterranean and Caribbean islands are suffering from an acute shortage of drinking water (El-Nashar, 2001). Water is becoming a matter of life and death, as more than one billion people around the world lack access to a steady supply of clean water, United Nations sources here told Gulf News recently. The sources cited Northern Africa and Western Asia (Arab countries) among the areas facing the most serious water shortages. While available amounts of water are

limited, the rate of population growth is high in the Arab countries, and noticeable expansion in the agricultural sector was recorded during the past few decades. The population of the 22 Arab countries, according to UN reports, is expected to reach 459.23 million by the year 2020 up from 281.22 million in 2000. By the year 2025, about 60% of the world population will be suffering from serious water shortages. Moreover, the common use of unhealthy water in developing countries causes 80–90% of all diseases and 30% of all deaths (Fath, 2000). For instance, water supply and sanitation in Saudi Arabia (Arabian Gulf Country) is characterized by challenges and achievements regarding to water challenges and issues. One of the main challenges is water the scarcity. To overcome water scarcity in Saudi Arabia, substantial investments have been undertaken in seawater desalination, water distribution, and wastewater treatment. Today, in Saudi Arabia, about 50% of drinking water comes from desalination, 40% from the mining of non-renewable

* Corresponding author.

E-mail addresses: whmfwelt@gmail.com (A. Almtairi), mohammed.eldeen@suezuniv.edu.eg, mwahab31@yahoo.com (M.A. Sharaf Eldean), amsoliman@ju.edu.sa (A.M. Soliman), aaboukhlewa@hbku.edu.qa (A. Mabrouk), h_elbanna_f@yahoo.com (H.E.S. Fath).

<https://doi.org/10.1016/j.clet.2021.100213>

Received 14 January 2021; Received in revised form 29 June 2021; Accepted 5 July 2021

Available online 8 July 2021

2666-7908/© 2021 The Authors. Published by Elsevier Ltd. This is an open access article under the CC BY license (<http://creativecommons.org/licenses/by/4.0/>).

groundwater, and only 10% from surface water in the mountainous southwest of the country (Walid, 2007). Among the achievements is a significant increase in desalination, and in access to water, the expansion of wastewater treatment, as well as the use of treated effluent for the irrigation of urban green spaces, and agriculture (Walid, 2007). Saudi Arabia is considered the largest producer of desalinated water in the world. In 2011 the volume of water supplied by the country's 27 desalination plants at 17 locations was 3.3 million m³/day (1.2 billion m³/year) (Abdullah, 2012). Six plants are located on the East Coast and 21 plants on the Red Sea Coast. Twelve plants use multi-stage flash distillation (MSF), and 7 plants use multi-effect distillation (MED). Both MSF and MED plants are integrated with power plants (dual-purpose plants), using steam from the power plants as a source of energy (Khulood et al., 2017). Eight plants are single-purpose plants that use reverse osmosis (RO) technology and power from the grid. By far the largest plant in 2012, Jubail II on the East Coast, is an MSF plant built in subsequent stages since 1983 with a capacity of almost 950,000 m³/day that supplies Riyadh city. The largest RO plant in 2012 was in Yanbu on the Red Sea coast. It supplies the city of Medina and has a capacity of 128,000 m³/day (Al-Harbi, 2011). Mecca city receives its water from plants in Jeddah and Shoaiba, just south of Jeddah. Ras al Khair, the largest plant of the country with a capacity of 1 million m³/day was opened in 2014, using RO technology (Arabnews, 2010). Regarding the existence of large capacities desalination plants in KSA, there is another side of desalination is that it is considered as high-energy consumption. Moreover, water and energy are the issues of this millennium. Therefore, applying nonconventional sources of energy integration technologies, especially geothermal energy in groundwater and seawater desalination considered a key proponent to meet the future of water shortage challenges. Nonconventional sources of energy have a potential advantage that is considered environmentally friendly besides, it can serve in arid and semi-arid regions. Generally, there are many studies that addressed economics of the desalination processes and the linkage between water desalination and new and renewable energies. Most of it were concentrated on the economics of desalination processes. It was found that solar, wind, geothermal, and wave energy can be used for the assistance of desalination technology in a general manner. For instance (M. Oulhazzan et al., 2016), studied the possibility of using linear Fresnel concentrators to reach up to 200 °C for vertical MSF desalination in Moroccan Sahara. (Mabrouk et al., 2007), and (Nafey et al., 2006) presented a thermo-economic technique of modelling related to different thermal desalination process (Mabrouk et al., 2007). and (Nafey et al., 2006) presented a viable economic analysis that can decide the cost of energy through the desalination process. In the same regard (Abdel Nasser Mabrouk et al., 2013), analyzed the effect of using the Nanofiltration (NF) with the MSF for high performance results. For the tri hybrid reverse osmosis (RO), forward osmosis (FO) and MSF processes (Abdel Nasser Mabrouk et al., 2017), presented a thermo-economic analysis based on real operating conditions. The results showed that the RO-FO-MSF process recovery ratio is 30% higher than that of the standalone RO and MSF processes. The specific total energy consumption, (electrical plus equivalent thermal) of the tri hybrid process is 65% lower than that of MSF, but 20% higher than RO (Darwish et al., 2015). investigated economically the possibility of utilizing solar photovoltaics and concentrated solar power (CSP) with different desalination processes. The study showed that using the thermally generated energy from concentrated solar collectors is much cheaper than using this thermal energy when directly operating the desalination system (Iaquaniello et al., 2014). investigated thermally and economically the use of CSP technology for hybrid MED/RO desalination process. The proposed system is aimed to produce 20,592,000 m³/year via solar energy (Soliman et al., 2020). presented an economic investigation about solar hydro power for reverse osmosis under Libyan operating condition. The results showed that the total water price was in the range of 0.65\$/m³. It is also shown by literature that geothermal energy can power thermal and electrical desalination systems as

presented by solar desalination. Geothermal desalination is particularly important for the locations where have a high scarcity of freshwater. It can serve against solar desalination when the field area is compared. Another advantage of geothermal power is that it is a non-intermittent resource, which means that energy can be produced continuously without interruption except during the maintenance of power plants (Østergaard and Lund, 2011). presented a technical scenario which described and developed the transition of Frederikshavn's city (Denmark) energy supply from being predominantly fossil fueled to being fueled by locally available renewable energy sources particularly by the aid of geothermal energy (Rosiek and Batles, 2012). had described a shallow geothermal system that was designed as an alternative to the cooling tower in a solar-assisted air-conditioning system which is installed in southern Spain (Almería). The results had demonstrated that during one cooling period, the seasonal shallow geothermal system uses 31% less electrical energy than a cooling tower system (Karytsas et al., 2003). presented a socio-economic study of the possible use of low enthalpy geothermal resources for district and greenhouse heating in the Traianoupolis Evros region (Greece). The thermal energy potential of the Traianoupolis geothermal field has been estimated at 10.8 MW_{th}. Techniques of geothermal desalination are many and varying according to the size of the demand for freshwater and the size of solar energy presence (Seyed Mojtaba Alirahmi et al., 2020). introduced a multi-generation system based on geothermal energy and parabolic trough solar collectors. The proposed system was designed to produce enough power via the Rankine cycle and an organic Rankine cycle for the reverse osmosis desalination plant. (Bouchekima B, 2003) analyzed the performance of solar still using geothermal sources in South Algeria with maximum temperatures of 60–70 °C (Bourouni K et al., 1999). demonstrated an aero-evapo-condensation process which was found to be promising for cooling as well as for desalting geothermal water. A brackish water greenhouse desalination process powered by geothermal energy source was proposed by (Mahmoudi et al., 2010). An integrated configuration including a multi-effect boiling unit and an MSF unit was evaluated in a feasibility study utilizing geothermal sources in Baja California, Mexico (Rodriguez et al., 1996). The geothermal source was available as a heat source for 80 °C (Francesco Calise et al., 2016). introduced a combination of the solar and geothermal poly-generation system for desalination purposes. The system supplies a small community with electricity, desalinated water, space heating and cooling through a district network. That hybrid multi-purpose plant was investigated based on an Organic Rankine Cycle (ORC) supplied by medium-enthalpy geothermal energy and by solar energy (Savvina Loutatidou et al., 2015). presented low enthalpy geothermal resources as a preliminary evaluation as a suitable desalination technology. The desalination processes are chosen, multiple effect distillation (MED) and reverse osmosis (RO) were designed as integrated energy-water systems (Rosalam Sarbatly et al., 2013). investigated the energy evaluation of the cross-flow vacuum membrane distillation (VMD) for desalination by the aid of geothermal energy. An economic analysis for a 20,000 m³/d VMD desalination plant finds that the water production costs are \$0.50/m³ and \$1.22/m³, respectively (Flavio Manenti et al., 2013). dealt with the parametric simulation for design and optimization purposes of a heat integrated geothermal desalination plant for domestic use of freshwater, focusing on the appealing multi-effect distillation (MED) process to handle water shortage in remote locations with low-temperature geothermal potential. The main driving thermal power was the free salt steam through the 1st effect of the MED process without any existence to the brine steam (Barbara Tomaszewska et al., 2013). studied the BWRO-membrane equipped desalination system that been achieved with geothermal waters containing 7 g/L TDS and a boron concentration of up to 10 mg/L (Amin and Mehrpooya, 2017) evaluated a Kalina cycle coupled to a reverse osmosis system to provide heating, cooling, power, and potable water by the aid of geothermal energy. Hot geothermal water was used as a heat source in the Amin's system. The results show that the system can provide 46.77 kW power, 451 kW

heating, 52 kW cooling, and 0.79 kg/s potable water. It is clear from the literature that using geothermal energy for membrane and/or thermal desalination is still under the research activities. Moreover, most of the geothermal desalination processes in literature was centralized about generating electric power from the geothermal plant to serve thermal or membranes via the Rankine cycle. However, using geothermal energy as a direct brine heater for thermal desalination processes was not investigated before. Most of the literature presented the geothermal well (abandoned oil wells) to drive the desalination plant by using motive steam or even through the binary cycle based on Organic Rankine Cycle techniques. For instance (Younes [Noorollahi et al., 2017](#)), presented a numerical simulation about the steam generation for the use of multi effect distillation. The steam which is free from salt is used directly through the 1st effect of the desalination plant. No brine has been used as driving thermal power in that regard (Mohammad-Reza [Kolahi et al., 2020](#)). proposed two configurations of combined flash-binary geothermal systems for simultaneous power production and water purification. In Kolahi's work (Mohammad-Reza [Kolahi et al., 2020](#)), free slat steam has been used as a main driving thermal power via flash tank (Chitta [Sahana et al., 2021](#)). presented a supercritical CO₂ power cycle for power generation and desalination via humidification dehumidification process. In Chitta's work (Chitta [Sahana et al., 2021](#)), the geothermal power was only used through the heat exchanger as instead of the combustion chamber of the gas turbine cycle. The driving steam was also free of salt and no brine steam was used in Chitta's work. Moreover, the desalination part is operated via intermediate heat exchanger (S. [Salehi et al., 2018](#)). investigated two configurations of double-flash geothermal power plants. One is combined with water desalination and the other is integrated with absorption heat transformation and water desalination. The main purpose of investigated systems was the simultaneous generation of electrical power and distilled water (S. [Salehi et al., 2018](#)). had used salt free steam as a driving thermal power via geothermal well. It has been realized that the common idea from the literature that the main driving thermal power was the salt-free motive steam without any existence of using the brine as motive steam. Therefore, the novelty of this work has emerged from the three main considerations that never been addressed before.

- (i) The first is to pump saline water into the geothermal well for heat and enthalpy gain. The geothermal well will act as a brine heater beside the flash evaporation tank.
- (ii) The second is the use of direct steam to be condensed on the end condenser tubes for freshwater production. Therefore, medium temperature ranges would be enough through the current study.
- (iii) The third is to use nanofiltration unit as a salinity reduction stage before the pumping process into the geothermal well, and the use of U-tube heat exchanger through the well. Such uses would help to increase the lifetime of the geothermal well, tubes, and heat exchangers units.

Furthermore, the system is supposed to be established at the location of 26°34'10"N, 40°10'59"E (Al Shamli Saudi Arabia) for the research reasons under the supervision of Jouf University, Sakaka, Saudi Arabia. For that purpose, a developed process modeling has been performed. Thermal and cost analysis are presented to judge the system feasibility regardless the salinity effect on the underground environment. Furthermore, the greenhouse effect is also calculated and investigated. Also, the current work will address process modeling from the side of energy, cost, and sizing. Meanwhile, the effect of salinity gradients on the geothermal well will not be investigated in this study. The proposed case study is expected to produce an amount of freshwater within the range of 500–1500 m³/day which can be used to serve small villages, rural areas, nomad's spots, and/or army units. Real time process modeling has also been adopted to recognize the system performance along one year. Two different terms are considered for measuring the system design and cost. The 1st method is about salinity operating

conditions effect, while the 2nd method is related to the temperature operating conditions effect.

2. The proposed novel system

As demonstrated earlier, geothermal well can produce enough power which would be capable of producing steam for thermal desalination processes. The main approach of this study is to analyze the proposed system from the sides of thermodynamics and cost. In the current work, the proposed new system differs from the conventional desalination processes such as single-effect evaporation type if compared. [Fig. 1](#) shows the proposed system diagram that has been considered in this work. The proposed system components are geothermal well (5), pre-stage nanofiltration (3), pump (2), flash tank (7), and the condenser/heat exchanger (4). Seawater will be pumped through the condenser unit as cooling water for two purposes. The first is to use it as a cooling load for the condensation process to the steam coming from the flashing tank (7), and the second is to be preheated before pumping into the geothermal well (5). Geothermal well will act as a brine heater to increase the brine temperature before the stage of flashing. Meanwhile, the preheated seawater will go through the geothermal well to gain the required energy (enthalpy) as hot water. Hot water will then be pumped towards the flashing tank for the evaporation process under low pressure (condenser pressure) (6–8). The flash tank (7) will transform the hot water into generating steam (salt-free) to be condensed outside the condenser tubes (8, 4, 10). The salt-free steam (8) will then condensate over the condenser tubes releasing its energy to the cooling water then to be collected as freshwater in the accumulative tray (10). The rest of the feed mass flow rate and non-condensable solute will be drawn away back to the blowdown reservoir (9, 11). The pumping unit (2) is used for seawater pumping into the geothermal well and for overcoming the pressure losses through the system tubes. Nanofiltration (3) has been used as a pre-stage section before the condenser unit to reduce the salinity contents in the intake of saline water. Reducing the salinity concentration will increase the plant lifetime and save the geothermal well too. It is expected to reduce the feed salinity from 47,000ppm to a level of 2,000ppm which is remarkably expected to be suitable for the tubing system through the geothermal well. Moreover, a U-tube heat exchanger (Shabnam [Gharibi et al., 2018](#)) will be used to reduce the salinity effect through the geothermal well, hence, reducing the negativity to the environment to minimum levels. A U-tube downhole heat exchanger retrofitted to a borehole is the most common method used to harness the ground heat for process heating and/or desalination ([Lee and Lam, 2008](#)), ([Rees, 2015](#)). Hence, several studies have been conducted on the design and performance of vertical U-tube heat exchangers for the utilization of shallow geothermal energy. Usually, the well filled with a proper filling material called grout (i.e. water) which makes the heat transfer between the tube and the ground possible. Low temperature seawater (from (4) to (5) on [Fig. 1](#)) as a working fluid is injected into the well through the inlet of the U-tube and acquires the geothermal heat while flowing through the stainless-steel U-tube. The material of the pipes is stainless steel.

3. Assumptions and mathematical model

The modelling techniques are mainly distinguished by to major types which are the performance technique and the design technique (S. [Salehi et al., 2018](#)), (Shabnam [Gharibi et al., 2018](#)), and (Lee et al., 2008). For performance model, the productivity would be calculated based on the knowledge of area, size, and flow rates (the process is already existed). In design technique of modelling, the productivity is kept known to calculate the area, size, flow rates, and cost (the process is not existed yet). In this work, it becomes particularly important to specify the freshwater capacity, thence; the thermal load on the geothermal well will be calculated. Sequentially, the thermal load will calculate all unknown design specifications beside the cost calculation.

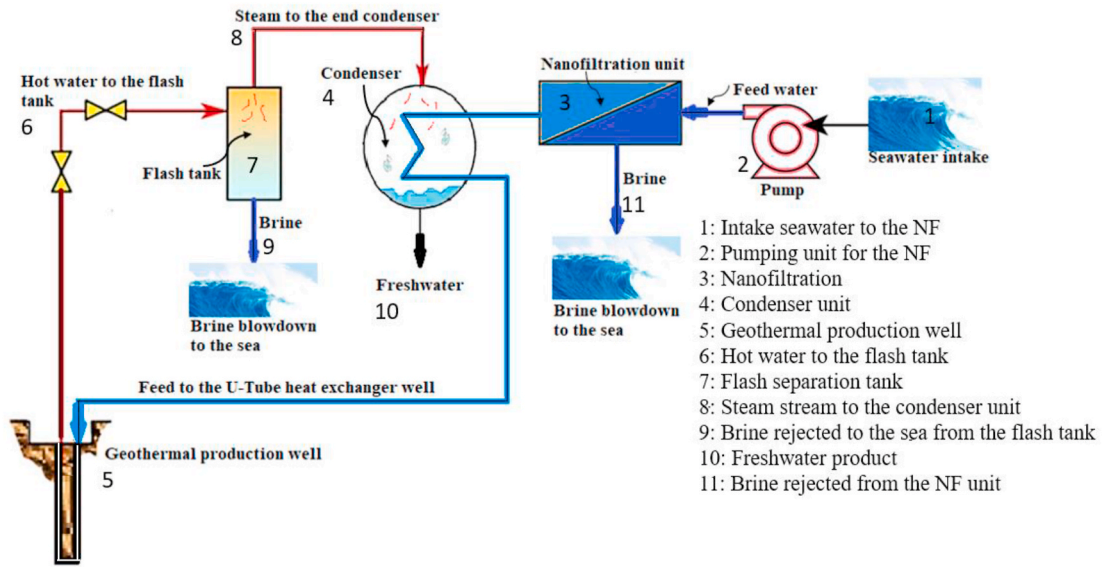


Fig. 1. A schematic diagram of the proposed system: Seawater intake, Nanofiltration, condenser/preheater, geothermal well, flashing tank, pump.

The unknown parameters are the areas, dimensions, mass flow rates, energy streams, cost streams, and the entire process temperatures or any other calculated physical properties. The following assumptions have been considered:

- The system goes under steady-state conditions.
- The system productivity is kept known and can be varying according to the consumption fluctuation in case of dynamic system or real time modeling.
- 365 epochs will represent one year of operation.
- Environmental operating conditions such as temperature, °C, or pressure are kept constant and can vary based on the case study.
- Flash tank dryness fraction will be calculated in design mode.
- Top cycle pressure will be assigned as an input.
- Pumps efficiency will be assigned in the range of 70%–75%.
- Condenser effectiveness will be assigned as 80%.

- Feed salinity will be set as 45,000ppm.
- Two methodologies will be adopted where the 1st is to run the model based on salinity operating conditions. While the 2nd is to run the model based on steam quality conditions. For the 1st case, the brine blow-down salinity (TDS) from the flash tank is assigned as an input and varying between 2000ppm and 20,000ppm. For the 2nd case, the steam quality will be assigned as an input and the brine blow down will be calculated. Moreover, in the 2nd methodology, steam temperature is lowered to minimum ranges (40–50 °C) to prevent scaling and deposits on the tubes.

Fig. 2 represents the model browser of the proposed system. As shown in Fig. 2, the proposed system has been simulated and connected (unit by unit) using MATLAB/Simulink toolbox. The system can be run in a dynamic/real time mode that simulates the real operating conditions based on the assumptions and data inputs or can be run based on

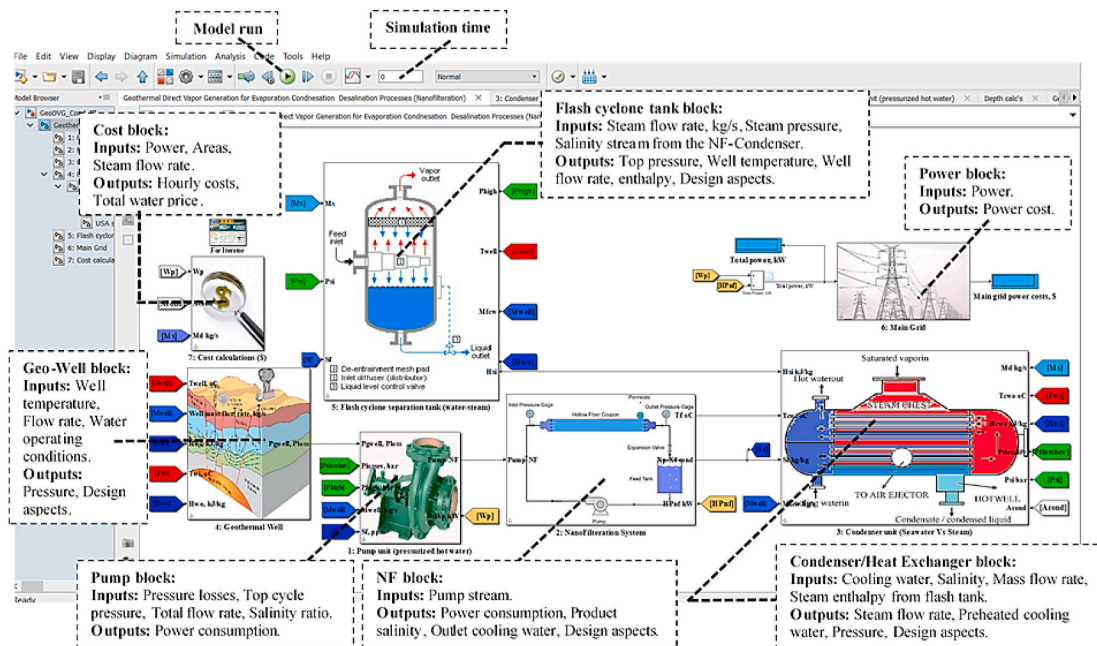


Fig. 2. The model browser of the proposed system under the MATLAB/Simulink environment.

static mode. The system runs based on iterative loop solution with forwarding and backward of entire streams. The system results will be examined under some important operating conditions such as productivity, steam quality, feed temperature and salinity changes. Beside thermodynamics and design aspects, hourly costs will be considered a valuable indicator to judge the system feasibility. Regarding the impact on the environment, the calculation of CO₂ emissions will take place in this work. The following subsections demonstrate the mathematical modeling of each unit of the proposed system.

3.1. The intake seawater

The type of saline water in this study is varying between brackish water salinity and/or seawater salinity. Ranges are varied between 1000ppm and 47,000ppm. Increasing the salinity ranges will increase the thermal load power on the pumping system. The density of the saline water is considered particularly important parameter which is varying based on temperature and salinity. Density, kg/m³ is calculated as presented in the following function by (A.S. Nafey and Sharaf, 2010), (Mohamed A. Sharaf Eldean and Soliman, 2013), and (M.A. Sharaf Eldean and Thesis, 2011).

$$\rho = (0.5 \times a_0 + a_1 \times Y + a_2 \times (2 \times Y^2 - 1) + a_3 \times (4 \times Y^3 - 3 \times Y)) \times 1000 \quad (1)$$

Where; ρ is the density in kg/m³, and Y is a functional parameter.

$$Y = \frac{2 \times T - 200}{160}, \quad T = \text{oC}$$

$$\sigma = \frac{(2000 \times S) - 150}{150}, \quad S = g / kg$$

$$a_0 = 2.01611 + 0.115313 \times \sigma + 0.000326 \times ((2 \times (\sigma^2)) - 1)$$

$$a_1 = -0.0541 + 0.001571 \times \sigma + 0.000423 \times ((2 \times (\sigma^2)) - 1)$$

$$a_2 = -0.006124 + 0.00174 \times \sigma + 0.000009 \times ((2 \times (\sigma^2)) - 1)$$

$$a_3 = 0.000346 + 0.00008 \times \sigma + 0.000053 \times ((2 \times (\sigma^2)) - 1)$$

Where, σ , and $a_{0...3}$ are functional parameters.

3.2. Nanofiltration section

The main role of the Nanofiltration in this study is to reduce the salinity contaminations effect on the tubes through the system. Lowering the salinity levels will reduce the scaling in the heat exchanger to the minimum levels specially while dealing with temperature ranges over 60 °C. In this work, the effect of the NF salt rejection (SR) parameter will be examined. The generated mathematical code for nanofiltration is presented as following by (M.A. Sharaf Eldean and Thesis, 2011). The number of nanofiltration (NF) units and be obtained by assigning the total plant productivity and the unit productivity:

$$NF_n = \frac{M_{pt}}{M_{p_{nf}}} \quad (2)$$

NF area, A_{nf} , m² is obtained based on diameter, ID_{nf} , m and length L_{nf} , m of the NF module:

$$A_{nf} = \pi \times ID_{nf} \times L_{nf} \quad (3)$$

The total NF area, m² would become:

$$A_{t_{nf}} = A_{nf} \times NF_n \quad (4)$$

Total feed flow rate M_f , kg/s is considered depending on total plant productivity M_{pt} , m³/day, operating hours, OH , and the recovery ratio, RR :

$$M_f = \frac{M_{pt} \times \frac{1000}{OH \times 3600}}{RR} \quad (5)$$

Thence, the total brine loss flow rate M_b , kg/s is then calculated:

$$M_b = M_f - \left(M_{pt} \times \frac{1000}{OH \times 3600} \right) \quad (6)$$

The permeate salinity, ppm is calculated based on feed salinity S_f , ppm, and salt rejection percentage, SR :

$$S_p = S_f \times (1 - SR) \quad (7)$$

The brine blowdown salinity, ppm can be obtained based on total productivity, feed and product salinities, S_f , S_p , ppm, feed, and brine flow rates (M_f , M_b), kg/s (M.A. Sharaf Eldean and Thesis, 2011):

$$S_b = \left(\frac{(M_f \times (S_f \times 1e - 6)) - \left(\left(M_{pt} \times \frac{1000}{OH \times 3600} \right) \times (S_p \times 1e - 6) \right)}{M_b} \right) \times 1e6 \quad (8)$$

Where, OH is the operating hours, hr. The average salt concentration, S_{av} , ppm by (Hisham T El-Dessouky and Ettouney, 2002) is then calculated:

$$S_{av} = \left(\frac{(M_f \times S_f \times 1e - 6) + (M_b \times S_b \times 1e - 6)}{M_f + M_b} \right) \times 1e6 \quad (9)$$

The pumping power required for filtration process is then obtained based on pressure difference across the filtration module.

$$HP = \frac{M_f \times \Delta P}{\rho(T_f, S_f) \times \eta_p} \quad (10)$$

Where, ρ , is the density, kg/m³, M_f is the feed flow rate and η_p is the pump efficiency. Thence, the specific power consumption, SPC , kWh/m³ is then calculated based on total plant productivity, kg/s, operating hours, OH , and the pumping power, HP , kW.

$$SPC = \frac{OH \times HP}{M_{pt}} \quad (11)$$

3.3. Condenser/heat exchanger

Two passes Surface Condenser is a device used to transfer heat between a steam and a fluid, or between two or more fluids. The fluids may be separated by a solid wall to prevent mixing, or they may be in direct contact. The condenser model should assign the cold side temperature, °C, hot side enthalpy, kJ/kg and steam mass flow rate, kg/s. Condenser thermal power, kW based on enthalpy difference between inlet and outlet, kJ/kg and mass flow rate of steam, M_{st} , kg/s is calculated as following (Hisham T El-Dessouky and Ettouney, 2002):

$$Q_{cond} = M_{st} \times (h_{cond_i} - h_{cond_o}) \quad (12)$$

By assigning the condenser effectiveness, inlet cooling water temperature, and hot side temperature, the outlet cooling water temperature, °C can be calculated:

$$T_{cw_o} = \epsilon_{cond} \times (T_{cond_i} - T_{cw_i}) + T_{cw_i} \quad (13)$$

Where, ϵ_{cond} is the condenser effectiveness. Cooling load mass flow rate, kg/s based on thermal energy and enthalpy difference on the cooling side can be calculated:

$$M_{cw} = \frac{\epsilon_{cond} \times Q_{cond}}{\Delta h_{cw}} \quad (14)$$

The outlet distillate temperature (liquid), °C can be calculated based on the effectiveness, ϵ_{conds} , cooling water temperature and inlet steam temperature, °C:

$$T_d = T_{si} - \varepsilon_{cond} \times (T_{si} - T_{cwi}) \quad (15)$$

Outlet enthalpy of the distillate water side (liquid), kJ/kg is obtained from the following correlation (M.A. Sharaf Eldean and Thesis, 2011), (Hisham T El-Dessouky and Ettouney, 2002):

$$h_d = 421.2 \times e^{(0.004008 \times T_d)} - 435.9 \times e^{(-0.007559 \times T_d)} \quad (16)$$

The outlet distillate pressure for water, bar, is calculated based on distillate temperature, °C (M.A. Sharaf Eldean and Thesis, 2011):

$$P_d = (2.407e - 09 \times T_d^{4.26}) + 0.199 \quad (17)$$

The overall heat transfer coefficient U_{cond} , kW/m²°C of the condenser is calculated as following (Hisham T El-Dessouky and Ettouney, 2002):

$$U_{cond} = 1e - 3 \times (1617.5 + 0.1537 \times T + 0.1825 \times T^2 - 0.00008026 \times T^3) \quad (18)$$

The non-equilibrium allowance NEA is calculated by the following equation (Hisham T El-Dessouky and Ettouney, 2002);

$$NEA = A + B \times T_d + C \times T_d^2 + D \times T_d^3 \quad (19)$$

Where $A=2.556$, $B= - 0.203 \times 10^{-1}$, $C= -0.129 \times 10^{-1}$ and $D= 0.1123 \times 10^{-5}$ are the functional parameters for the calculation of the NEA . Cold side heating capacity is then calculated (Incropera and DeWitt, 2002) based on liquid specific heat capacity, C_p , kJ/kg°C ($=f(T, S)$) and mass flow rate, kg/s:

$$C_{cold} = C_p(T, S_f) \times M_{cw} \quad (20)$$

Hot side heating capacity is then calculated (Incropera and DeWitt, 2002) based on steam specific heat capacity, kJ/kg°C ($=f(T, S)$) and mass flow rate, kg/s of the steam:

$$C_{hot} = C_p(T, S_p) \times M_p \quad (21)$$

Maximum and minimum heat capacities is then calculated C_{max} & C_{min} :

$$C_{max} = \max(C_{cold}, C_{hot}) \text{ \& } C_{min} = \min(C_{cold}, C_{hot}) \quad (22)$$

The capacity ratio C is then calculated:

$$C = \frac{C_{min}}{C_{max}} \quad (23)$$

Number of heat transfer unit based on number of passes (NOP) and effectiveness, ε_{cond} is found as following (Incropera and DeWitt, 2002):

$$E = \frac{\left(\frac{2}{\varepsilon_{cond}}\right) - (1 + C)}{(1 + C^2)^{0.5}} \quad (24)$$

$$NTU = NOP \times -1 \times (1 + C^2)^{0.5} \times \left(\log\left(\frac{E - 1}{E + 1}\right)\right) \quad (25)$$

Where, E is a functional parameter for the NTU . The heat transfer area, m² is then calculated:

$$A_{cond} = \frac{NTU \times C_{min}}{U_{cond}} \quad (26)$$

3.4. Pump

Pumping system is responsible for flowing the brine through the system. It is anticipated by this device to overcome all hydraulic losses through the proposed system. The model can go through the following calculations (M.A. Sharaf Eldean and Thesis, 2011):

The total pressure difference ΔP_{total} , bar:

$$\Delta P_{total} = P_{gwell} + P_{high} + P_{loss} \quad (27)$$

Where, P_{gwell} , P_{high} , and P_{loss} are the geothermal well head pressure, top cycle saturation pressure and tubes head losses pressure, respectively. The pump power W_p , kW is calculated where the pressure is in bar SI unit:

$$W_p = \frac{100 \times M_{total} \times \Delta P_{total}}{\rho(T_{well}) \times \eta_p} \quad (28)$$

Where, $\rho(T_{well})$ is density, kg/m³ as a functional of well temperature T_{well} , °C.

3.5. Geothermal well

Geothermal wells deeper than 100 m can be employed to power desalination plants. The geothermal energy would be used to heat the saline water and or it could be used to generate electricity for operating reverse osmosis units. Furthermore, with the recent progress thermal distillation technology, the utilization of geothermal brine with temperature up to 60 °C has become a promising option. Geothermal well is the most important part in this proposal. It will act as a brine heater and/or steam generator. To prevent leakage of the salinity to the geothermal well, a stainless-steel U-tube has been considered. The following relations govern the mathematical code for geothermal well (Gupta and Roy, 2007), (Ronald DiPippo, 2007). Silica, ppm and Sodium/potassium, SPR , ppm, concentrations @ well temperature °C are calculated as following:

$$Silica = 0.04097 \times T_{well}^{1.66} + 50.8 \quad (29)$$

Sodium/Potassium, Na/K, ratio (Gupta and Roy, 2007):

$$SPR = e^{\left(\frac{1217}{T_{well} + 273}\right) - 1.483} \quad (30)$$

Well pressure based on depth (km), bar:

$$P_{gwell} = 82.51 \times e^{0.3796 \times W_{Depth}} - 81.04 \times e^{-0.7998 \times W_{Depth}} \quad (31)$$

Where, W_{depth} is the well depth parameter in km. Well head pressure, WHP , bar is calculated based on the well mass flow rate M_{well} , kg/s:

$$WHP = -3.746e - 05 \times e^{0.1124 \times M_{well}} + 21.61 \times e^{-0.002908 \times M_{well}} \quad (32)$$

Number of injection wells (Ronald DiPippo, 2007):

$$NOIW = \frac{M_{well}}{16} \quad (33)$$

Number of suction wells (Ronald DiPippo, 2007):

$$NOSW = \frac{M_{well}}{8.5} \quad (34)$$

Pressure loss due to friction through the piping system, bar can be calculated based on the following parameters:

$Re = \left(\frac{4}{\pi}\right) \times \left(\frac{M_{well}}{D_{pipe} \times \mu(T_{well})}\right)$ where, Re is the Reynold's number, M_{well} is mass flow rate through the well, kg/s, D_{pipe} is the well pipe diameter, m, and $\mu(T_{well})$, is the fluid viscosity, Pa.s, as a function of well temperature, T_{well} , °C.

$A_{pipe} = \left(\frac{4}{\pi}\right) \times D_{pipe}^2$, where A_{pipe} is the cross-sectional area, m².

$V_f = \frac{M_{well}}{\rho(T_{well}) \times A_{pipe}}$, V_f is the flow velocity through the piping system, m/s.

$$P_{loss,well} = \frac{\left(f \times \left(\frac{1000 \times W_{Depth}}{D_{pipe}}\right) \times \rho(T_{well}) \times \left(\frac{V_f^2}{2}\right)\right)}{100000} \quad (35)$$

Where, $f = 64/Re$ is the friction coefficient. Well hole inch, m can be calculated from the following correlation based on well depth, ft

(Ronald DiPippo, 2007):

$$D_{hole} = \left(-19.41 \times \left(W_{Depth_p}^{0.1266} \right) \right) + 77.31 \quad (36)$$

Digging casing diameter, inch based on well depth in, ft (Ronald DiPippo, 2007):

$$D_{case} = \left(-56.72 \times \left(W_{Depth_p}^{0.05821} \right) \right) + 109.1 \quad (37)$$

3.6. Flash tank

Flash cyclone tank or flash evaporation tank is used in this study as a steam generator, where the sudden decrease in pressure causes the liquid water to “flash,” or vaporize, into steam. In this process, geothermally heated water is drawn up through a different set of pipes, and much of the energy stored in the heated water is transferred to the working fluid through a condenser/heat exchanger. Meanwhile, the vapor from the working fluid passes through the surface condenser for the desalination part i.e., condensation and freshwater production. The process model is presented as the following (Ronald DiPippo, 2007). The steam tube cross sectional area, A_t , m^2 is calculated based on steam mass flow rate, kg/s , vapor density, kg/m^3 and steam vapor velocity, m/s .

$$A_t = \frac{M_{st}}{\rho_v \times V_{st}} \quad (38)$$

Where, ρ_v is the vapor density in kg/m^3 . The flash tank height, H_{fsh} , m is calculated based on the tube diameter, m :

$$H_{fsh} = 7.15 \times D_t \quad (39)$$

Flash tank width, m :

$$W_{fsh} = 3.5 \times D_t \quad (40)$$

Flash tank total volume, m^3 :

$$Vol_{fsh} = \left(\frac{\pi}{4} \right) \times W_{fsh}^2 \times H_{fsh} \quad (41)$$

Flashing enthalpy is equal to the well enthalpy coming from the geothermal well, kJ/kg :

$$h_{fsh} = h_{well} \quad (42)$$

The flashing dryness fraction, X_{fsh} is calculated based on flashing enthalpy, h_{fsh} , liquid enthalpy, h_f , and dry vapor enthalpy h_g , kJ/kg :

$$X_{fsh} = \frac{h_{fsh} - h_f}{h_g - h_f} \quad (43)$$

Total mass flow rate, kg/s :

$$M_{total} = \frac{M_{st}}{X_{fsh}} \quad (44)$$

Water content flowrate at the bottom of the tank, kg/s :

$$M_w = (1 - X_{fsh}) \times M_{total} \quad (45)$$

3.7. Cost analysis

For cost analysis, the amortization factor should be calculated first by (M.A. Sharaf Eldean and Thesis, 2011), $1/y$, $A_f = \frac{i \cdot (1+i)^{LT_p}}{(1+i)^{LT_p} - 1}$ where LT_p is the plant lifetime, and i is the interest rate, %.

- Geothermal investment cost, \$ is set as 900–1000\$/kW of power consumption (Ronald DiPippo, 2007). Therefore, the indirect capital cost is calculated as $IC_{gwell} = 900 \times W_p$, and the total annual costs, \$/y is $TAC_{gwell} = IC_{gwell} \times A_f$, therefore, the hourly costs are \$/h,

$$Z_{gwell} = \frac{TAC_{gwell}}{OH \times 365} \quad (46)$$

- Flashing tank cost is calculated based on the total tank volume correlation, \$, $IC_{fsh} = \frac{Vol_{fsh} \times 6.3e3}{3.8}$, hence, the total annual cost, \$/y is then calculated $TAC_{fsh} = IC_{fsh} \times A_f$, and the hourly costs are calculated, \$/h,

$$Z_{fsh} = \frac{TAC_{fsh}}{OH \times 365} \quad (47)$$

- The condenser cost parameters (IC_{cond} , TAC_{cond} , Z_{cond}) are calculated based on the total condenser area, where $IC_{cond} = 150 \times A_{cond}^{0.8}$, is the investment cost, \$. Hence, the total annual cost, \$/y is then calculated based on the investment cost, $TAC_{cond} = IC_{cond} \times A_f$, and the condenser hourly cost Z_{cond} , \$/h is then calculated based on the total annual cost in \$/h as

$$Z_{cond} = \frac{TAC_{cond}}{OH \times 365} \quad (48)$$

- The pump investment cost is calculated based on the pumping power, W_p , kW, $IC_p = 3500 \times W_p^{0.47}$. Hence, the total annual cost, TAC_p , \$/y is then calculated $TAC_p = IC_p \times A_f$, and hourly cost parameter, Z_p , \$/h is calculated based on the total annual cost parameter,

$$Z_p = \frac{TAC_p}{OH \times 365} \quad (49)$$

For Nanofiltration, membrane replacement cost parameter (MRC) (M.A. Sharaf Eldean and Thesis, 2011) is ranged as $MRC=30-60\$/m^2$. By knowing the total area of the NF , the membrane replacement cost can be calculated as following:

$$MRC = 30 \sim 60 \times A_{nf} \quad (50)$$

Calculation of fixed costs TFC , \$ based on fixed cost related to MRC , setup costs, and power cost:

$$FC = 2.55 \times MRC \quad (51)$$

Setup membranes costs, MC , \$:

$$MC = 0.5 \times MRC \quad (52)$$

NF pumping cost, PC_{nf} , \$:

$$PC_{nf} = 3500 \times HP^{0.47} \quad (53)$$

$TFC=FC + MC + PC_{nf}$

Calculate the total variable costs, TVC , \$ which are energy, EC , cleaning, $Clean$, and labor costs, LC :

$$EC = 0.5 \times MRC \quad (54)$$

$$Clean = 0.25 \times MRC \quad (55)$$

$$LC = 2 \times MRC \quad (56)$$

$$TVC = MRC + EC + Clean + LC \quad (57)$$

The total capital costs of the NF , \$ is then calculated as the summation of variable and fixed costs $TCC_{NF}=TVC + TFC$. The annual capital costs of the NF , \$/y is then calculated as $TAC_{NF} = TCC_{NF} \times A_f$. For the whole system, the total hourly costs \$/hr is then calculated based on all parameters as following, $Z_{tot} = Z_{gwell} + Z_{fsh} + Z_{cond} + Z_p + Z_{NF}$. Total Plant Costs is also calculated based on the total annual costs for all unit, \$/y, $TPC = TAC_{gwell} + TAC_{fsh} + TAC_{cond} + TAC_p + TAC_{NF}$

Total water price, \$/m³ can be calculated based on total plant cost parameter or via hourly costs.

$$TWP = \frac{TPC}{M_{pt} \times 365 \times LF} \quad (58)$$

Where, LF is the load factor.

3.8. Greenhouse gas (GHG) analysis

Greenhouse gases (GHG) emissions are a valuable indicator of system performance regarding environmental impact. More thermal desalination plants would probably increase GHG emissions. In this study, GHG is calculated for the adopted system to measure the impact on the environment. The GHG indicator is based on considerations obtained from the literature (Jia et al., 2019), (Burkhardt et al., 2012), (Nordin et al., 2013) (Cornejo P.K et al., 2014), and (Serhat Akin et al., 2020). For simplicity, this study focused on CO_2 generation as a representative GHG indicator. In this work, emissions resulting from energy consumption for the entire desalination system are considered for the CO_2 indicator. Emissions related to inlet feed stream and outlet reject brine are neglected as they are minor compared to emissions from energy consumption. The total emission EM_t is calculated based emissions from the geothermal well and the NF section, $EM_t = EM_{Geo} + EM_{NF}$, tCO_2/y . The desalination emissions can be expressed as following:

$$EM_{NF} = (P_e + P_{th}) \times OH \times \left(\frac{EM_{fd} = 1.04}{1000} \right)$$

where, OH , hrs, is the operating hours, EM_{fd} (Jia et al., 2019) is the emission factor for desalination (~ 1.04 tCO_2/MWh (Jia et al., 2019), (Cornejo P.K et al., 2014)) and P_e , kW, is the power consumption (auxiliaries, pumps, facilities, etc ...) and P_{th} the thermal power, kW. EM_{Geo} is the geothermal well emission and it is calculated as following:

$$EM_{Geo} = P_{th} \times OH \times EM_{fGeo} \times 10^{-6}$$

where P_{th} is the thermal power, kW, OH is the operating hours, and EM_{fGeo} is the emission factor for the geothermal part (~ 121 gCO_2/kWh (Serhat Akin et al., 2020)).

4. Results and discussions

For the proposed system, it is particularly important to assign the system performance parameters and operating conditions that should calculate an optimized result. In this part, two different methods have been thermally adopted to measure the design and performance aspects of the proposed system. The 1st condition is to measure the effect of salinity ratio on the system performance at high temperature rates. The 2nd condition is to measure the operating conditions such as temperature and steam quality on the system design and performance. System optimization will lead to assign and recommend the best operating conditions to judge the system cost and water price.

4.1. Salinity & operating conditions effect

For the current effect, the system initial conditions are listed as following:

- Feed salinity is 45,000ppm, and the brine blowdown from the flashing tank is set as in the range of 2500-15,000ppm.
- Recovery ratio is set as 30%.
- Salt rejection percentage is set as 90–95%.
- NF module productivity is set as $45m^3/day$.
- Pumps efficiency is set as 75%.
- Total productivity was in the range of 500–1500 m^3/day .

The result will be targeting the following indicators:

- Total water price, $\$/m^3$.

- Dryness fraction.
- Well depth, km.

Fig. 3 shows the effect of total plant productivity and top steam temperature on total water price, TWP, $\$/m^3$ and geothermal well depth, km parameters. From the figure, the influence of the system productivity has no significant effect. While, increasing the steam temperature (T_s , $^{\circ}C$) would cause more costs and more depth too. For instance, at 500 m^3/day and 100 $^{\circ}C$, the TWP, $\$/m^3$ has found as 0.24 $\$/m^3$ (see Fig. 3-a) and the geothermal well depth was in the range of 3.3 km (see Fig. 3-b). While at 500 m^3/day and 200 $^{\circ}C$, the TWP, $\$/m^3$ has been recorded in the range of 1.6–1.7 $\$/m^3$ with a total well depth of 5.3 km. Meanwhile, the steam temperature value should be selected carefully because it has a massive effect on the system design and cost. Therefore, a value of 100 $^{\circ}C$ and productivity range of 500–1500 m^3/day are considered an optimized range that should be operated in this work. Such consideration would achieve a minimum cost ranges of 0.24–0.25 $\$/m^3$ and minimum well depth in the range of 3.4 to 3.5 km. Fig. 4 represents the effect of salinity ratios (feed & brine, ppm) on the TWP, $\$/m^3$, dryness fraction, and the geothermal well depth. The result data on the Fig. 4 has been recorded based on 500 m^3/day and 100 $^{\circ}C$ of steam temperature. Fig. 4-a shows that by decreasing the feed salinity S_f , ppm, the TWP, $\$/m^3$ would increase. For instance, at feed salinity $S_f=45,000$ ppm and brine salinity $S_b=2500$ ppm, the TWP was recorded as 0.2 $\$/m^3$. However, at $S_f=25,000$ ppm and $S_b=2500$ ppm, the TWP is equal to 1.25 $\$/m^3$ i.e. the percentage of increase was 5.25%. Therefore, it will be highly recommended to operate the system at high salinity ratios related to the feed salinity.

The reason of that was referring to the reduce of the feed salinity which will reduce the salinity ratio of the stream goes towards the geothermal well. However, increasing the brine blowdown salinity S_b , ppm would increase the TWP, $\$/m^3$. Both parameters have a direct effect on the brine blowdown flow rate from the flash tank design aspects which probably will effect on the dryness fraction parameter. Therefore, it will be highly recommended to assign the feed salinity at a value of 45,000 ppm and brine blowdown at a value of 2500ppm to achieve minimum TWP, $\$/m^3$ (0.24). However, that would operate the system at minimum levels of dryness fraction ($\sim 10\%$ of steam) which is not recommended. Fig. 4-b shows that by increasing the brine blowdown salinity ratio, the dryness fraction will increase. Increasing the percentage of dryness fraction is favorable however, it will increase the system cost values. Therefore, to achieve suitable rates of steam with minimum ranges of TWP, $\$/m^3$ and well depth, km (see Fig. 4-c), it is highly recommended to assign the brine blowdown at 5000ppm. This will lead to at least a range of 50% increase in dryness fraction (steam quality) which is highly recommended. Reducing the feed salinity will increase the dryness fraction too. However, it will increase the TWP, $\$/m^3$, and well depth, km parameters as well. For instance, the well depth, km (see Fig. 4-c) will increase by 8% in case of the operation at feed salinity equal to 25,000ppm. The brine blowdown also will cause a massive increase in dryness fraction and well depth. For instance, the percentage of increase would become 60% at $S_b=15,000$ ppm (from 3.3 up to 8.5 km). Maximum allowable dryness fraction can be obtained at $S_f=25,000$ ppm and $S_b=15,000$ ppm.

However, the TWP, $\$/m^3$ and well depth parameters will increase dramatically to become 1.4 $\$/m^3$ and 8.7 km, respectively. Therefore, a value of $S_b=5000$ ppm is highly recommended in this work. Fig. 5 shows the effect of total plant productivity and salt rejection percentage on the TWP, $\$/m^3$, dryness fraction, and well depth, km parameters. Fig. 5-a shows that by increasing the plant productivity, a slightly decrease will be noticed on the TWP values. A significant change on the TWP will be caused by the salt rejection (SR) parameter related to the NF operation. Increasing the salt rejection percentage from 0.9 up to 0.95 will increase the TWP from 0.24 $\$/m^3$ @ 500 m^3/day up to 1.37 $\$/m^3$. The same behavior has been noticed on the dryness fraction which has been increased from 10% up to 55% at 0.95 of SR value (see Fig. 5-b).

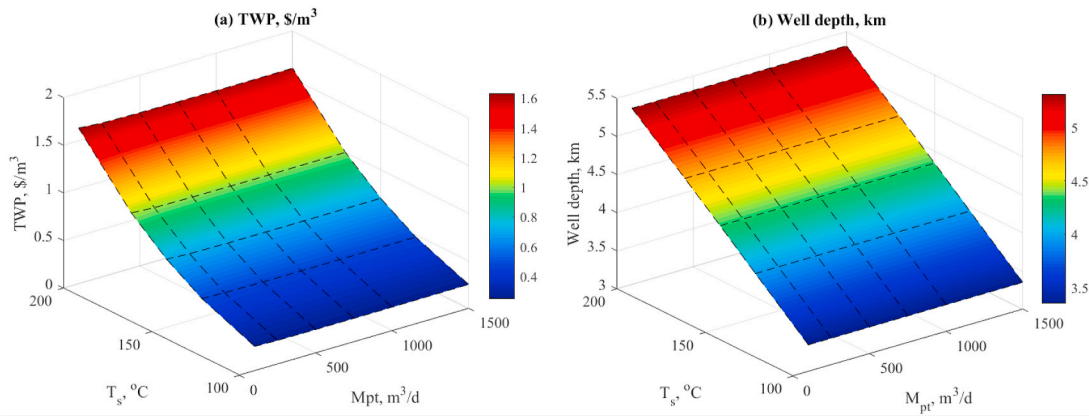


Fig. 3. The effect of total plant productivity and top steam temperature on (a) TWP, \$/m³, and (b) Geothermal well depth, km.

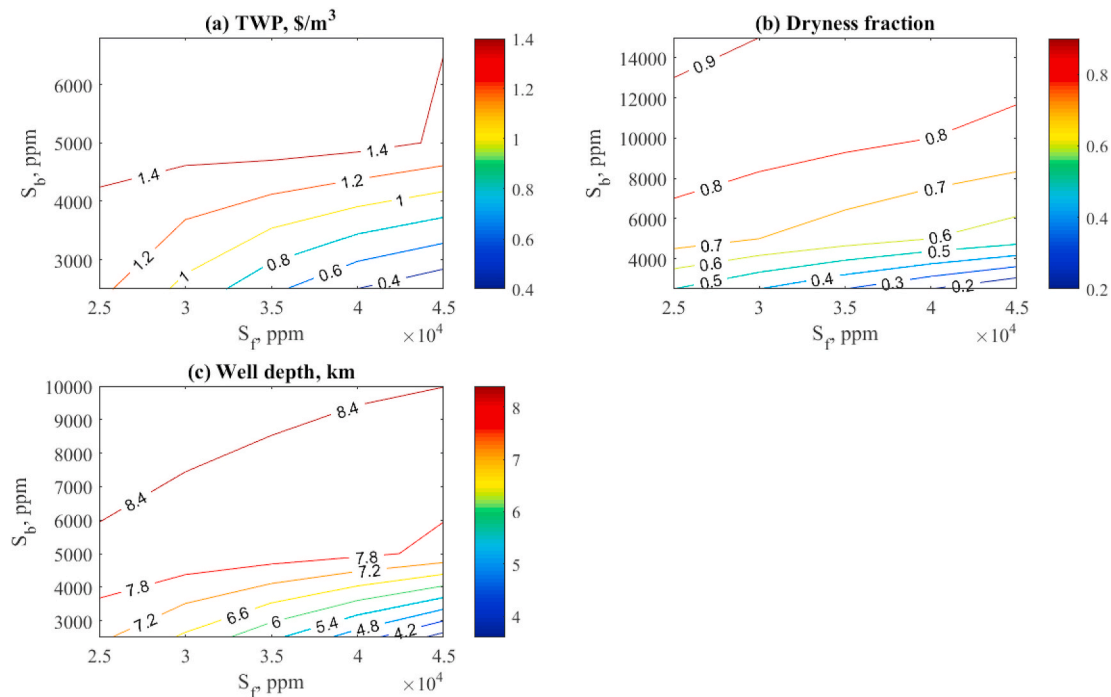


Fig. 4. The effect of salinity ratios on (a) TWP, \$/m³, (b) Dryness fraction, (c) Well depth, km. Data obtained @ 500m³/day & 100 °C.

Fig. 5-c shows the effect of SR and productivity parameters on the geothermal well depth. Increasing the SR percentage will increase the well depth which is not favorable. The percentage of increase has reached more than 56% related to the increase of SR from 0.9 up to 0.95. Therefore, to achieve best operating conditions putting in considerations the optimum well depth, dryness fraction and TWP, a value of 0.93 of SR should be considered beside 500m³/day as a total plant productivity. Based Fig's. 3–5, the following recommendations should be considered.

- Plant productivity should be in the range of 500–750m³/day.
- Top steam temperature should not exceed over 100–120 °C.
- Feed salinity should be in the range of 40,000–45,000ppm.
- Brine blowdown salinity should be set at the value of 4500–5000ppm.
- Salt rejection percentage should be set at the value of 0.93–0.95.

Generally, increasing the SR parameter will increase the dryness fraction however, it would increase the cost and the well depth too. The same behavior was noticed on the brine blowdown salinity and top

steam temperature parameters. Increasing the plant productivity will be considered the increase of the gain which will lead to a slightly decrease in total water price.

Based on the optimized indicators, it is quite important to discover the behavior of the system under the dynamic modeling operating conditions. The fluctuations of system productivity, salinity, salt rejection percentage, top steam temperature and brine blowdown salinity will probably effect on the system performance. Data results were obtained along one year based on the fluctuations of that mentioned indicators. Table 1 illustrates the data results that been obtained based on the model data assumptions related to this study. Table 1 shows that the pumping power was in the range of 200 kW which is considered relatively high due to the high rate of flow through the cycle.

Meanwhile, the specific power consumption, SPC, kWh/m³ for the nanofiltration unit is considered high within the range of 8-9 kWh/m³. That because of the high ranges of salinity concentration. The average number of NF unit would be 60–80 units with total area about 40–50 m². The condenser area will be in the range of 70 m² with 1111 tubes and 10 passes. Condenser tube length would be 1.5m. For geothermal well, the

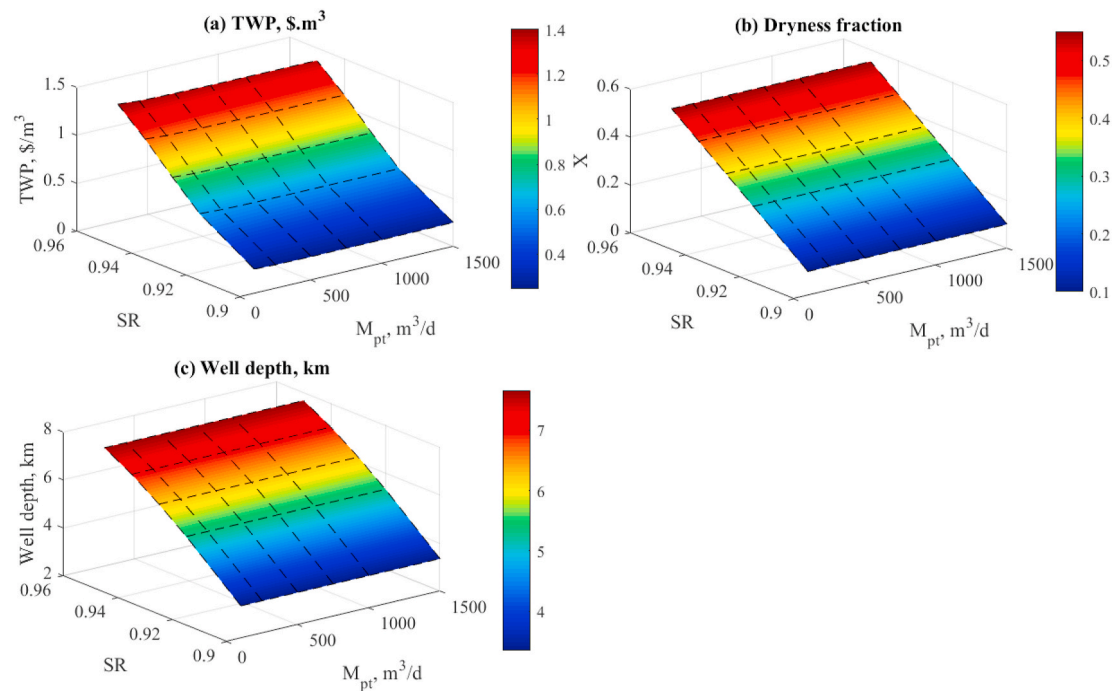


Fig. 5. Effect of plant productivity and salt rejection percentage on (a) TWP, $\$/\text{m}^3$, (b) dryness fraction, (c) well depth, km at $S_b=5000\text{ppm}$, $S_f=45,000\text{ppm}$, $T_s=100^\circ\text{C}$.

well depth was 7 km which is considered to obtain 320°C . Such temperature range is considered typically proportional with the depth at the location of operation.

The well total flow rate was about 13 kg/s which is considered a moderate range and suitable for such systems in case of no power generation will be needed. Total hourly costs were in the range of $2\$/\text{h}$ where the geothermal well was recorded as much greater among the other units. As expected, pumping units consumed more power and that would cost $0.3\text{--}0.5\$/\text{h}$. The total water price is recorded as $1.2\$/\text{m}^3$ which is considered relatively high while comparing against reverse osmosis. However, it can compete against multi-stage flashing related to that value.

Fig's. 6, 7 represents the dynamic behavior of the proposed system along one-year (365 epochs) of operation period. Related to the cost indicators, Fig. 6 shows the fluctuations of the hourly costs and total water prices parameters for each unit. Fig. 6-a shows that the total hourly cost parameter is fluctuating around $2\text{--}2.5\$/\text{h}$. While the geothermal hourly cost was in the range of $1\text{--}2\$/\text{h}$. The figure indicates that geothermal well is considered most costly if compared against the other units. However, the total hourly costs within the range of $2\$/\text{h}$ is considered a remarkable result while comparison against the conventional desalination processes. The fluctuations are little bit high due to the change in steam temperature and the brine blowdown salinity variations. Fig. 6-b shows the deviation between the total hourly costs and pumping unit hourly cost. The pumping hourly cost was in the range of $0.3\text{--}0.4\$/\text{h}$ which is considered relatively high by 20% of the total hourly costs. Condenser hourly cost is found as 1.5% (see Fig. 6-c) of total hourly costs because of the limited condensation area that been used. Fig. 6-d shows the fluctuations of the total water price parameter along one year. The range was fluctuating between 0.7 and $1.4\$/\text{m}^3$. Such values can compete against the conventional desalination processes in the same production category. Fig. 7 shows the design aspects related to the fluctuations of the system operating conditions along one year. Fig. 7-a shows the fluctuations in mass flow rates across the cycle. The total cycle flow rate is ranged between 12 and 20 kg/s. While the brine blowdown was in the range of 10 kg/s. Fig. 7-b represents the fluctuation in top well temperature along one year. As it can be shown

from Fig. 7-b, the average value was in the range of 300°C which is considered high, and it will need more depth into the ground. Minimum well temperature levels were in the range of 260°C . The same behavior was noticed on Fig. 7-c which represents the well head pressure. It was fluctuating between 45 and 50 bar. Silica concentration was noticed in the range of 500ppm to 700ppm (see Fig. 7-d). It is a directly affected by the well temperature and the depth of the well. Brine blowdown salinity is compared to the average salinity on Fig. 7-e. Fig. 7-f shows that the geothermal well depth was varying according to the well temperature variation. It is expected to reach to 300°C at the depth of 7 km.

4.2. Steam quality & operating conditions effect

The problem with the previous method is that the salinity may cause a severe corrosion on the system tubes specially at high ranges of feed and steam temperature. Therefore, in this method, the steam quality and operating conditions will be responsible for the design results under normal rates of salinity and temperature ranges. For instance, the steam temperature will be assigned in the range of 40 to 50°C which is considered low in this regard. The following considerations were taken as a system operating condition:

- Feed salinity is $44,000\text{--}45,000\text{ppm}$.
 - Recovery ratio is set as 30%.
 - Salt rejection percentage is set as 93–95%.
 - NF module productivity is set as $45\text{m}^3/\text{day}$.
 - Pumps efficiency is set as 75%.
 - Total productivity was in the range of $500\text{--}1500\text{m}^3/\text{day}$.
 - Dryness fraction was in the range of 10–50%.
 - Top steam temperature is ranged between 40 and 50°C .
- The result will be targeting the following indicators:
- Total water price, $\$/\text{m}^3$.
 - Brine blowdown salinity from the flashing tank.
 - Well depth, km.
 - Total hourly costs, $\$/\text{h}$.

Fig. 8-a, b, c, d show the variations of the input data that have a

Table 1
Data results of the proposed system based on the optimized design indicators.

| | |
|--|-----------|
| Pump unit: | |
| Flow rate, kg/s | 13.72 |
| Pressure losses, bar | 0.01–0.05 |
| Top pressure, bar | 113.4 |
| Power, kW | 207.5 |
| Nanofiltration unit: | |
| Membrane productivity/total, m ³ /day | 45/519 |
| Feed flow rate, kg/s | 1.91 |
| Brine blowdown, kg/s | 1.337 |
| Product salinity (to the well), ppm | 2653 |
| Brine salinity, ppm | 6.24e4 |
| Number of units, # | 60–80 |
| Total area/unit area, m ² | 50/0.648 |
| Power, kW | 18.4–20 |
| SPC, kWh/m ³ | 8.9–9 |
| MRC, \$ | 1296 |
| Membrane diameter, m | 0.2 |
| Membrane length, m | ~1 |
| Slat rejection, % | 94 |
| Condenser unit: | |
| Top steam temperature, °C | 115 |
| Steam enthalpy, kJ/kg | 2703 |
| Inlet cooling water temperature, °C | 20 |
| Outlet cooling water temperature, °C | 87.38 |
| Distillate temperature, °C | 51–52 |
| Steam flow rate, kg/s | 6.021 |
| Cooling water flow rate, kg/s | 13.72 |
| Cooling water salinity, ppm | 2653 |
| Condenser area, m ² | 67–70 |
| Number of tubes, # | 1111 |
| Tubes length, m | 1.5 |
| Thermal power, kW | 1.5e4 |
| Exergy destruction rate, kW | 2927–3000 |
| Geothermal well: | |
| Inlet flow temperature, °C | 87.38 |
| Well temperature, °C | 320.5 |
| Well inlet/outlet enthalpy, kJ/kg | 372/1465 |
| Well total flow rate, kg/s | 13.75 |
| Well depth, km | 7 |
| Digging pipe hole diameter, In | 8 |
| Digging pipe casing diameter, In | 7.3 |
| Number of injection wells/suction wells | 1/2 |
| Silica concentration, ppm | 642.2 |
| Salinity concentration, ppm | 2653 |
| Flash cyclone unit: | |
| Flashing enthalpy, kJ/kg | 1465 |
| Total flow rate, kg/s | 13.72 |
| Brine content flow rate, kg/s | 7.7 |
| Dryness fraction, % | 43.88 |
| Tank volume, m ³ | 11.4 |
| Tank height, m | 5 |
| Tank width, m | 1.7 |
| Drain, m | 0.163 |
| Vent, m | 0.6 |
| Cost analysis: | |
| Geothermal well hourly costs, \$/h | 1.642 |
| Condenser hourly costs, \$/h | 0.0355 |
| Pump hourly costs, \$/h | 0.348 |
| Nanofiltration hourly costs, \$/h | 0.207 |
| Total hourly costs, \$/h | 2.23 |
| Total water price, \$/m ³ | 1.206 |

remarkable effect on the system design and performance. The data are randomly selected and ascended from minimum to maximum values within the listed ranges that shown above in the assumptions section. Fig. 9 shows the data results based on the entry variables that been shown in Fig. 8. The variation has been selected based on productivity range from 500 to 1500m³/day. Fig. 9-a shows the variation of the total hourly costs at different productivity values. It was quite clear that 1500m³/day would record the highest values among the other values (500 & 750m³/day). That behavior was in decreasing mode according to the increase of the steam quality X, % or the top steam temperature. Therefore, it is quite important to increase the steam quality up to 30%.

There was no significant effect over the value of 30% of the steam quality X, %.

The total hourly cost was marked between 3\$/h @ 500m³/day and 7 \$/h @ 1500m³/day. The same decreasing behavior was noticed on Fig. 9-b related to TWP, \$/m³. However, increasing the productivity would decrease the TWP values from 0.16\$/m³ @ 500m³/day & 40% to 0.12\$/m³ @ 1500m³/day & 40%. Based on Fig's. 9-a, b, it is quite important to increase the system productivity however, the hourly costs will be increased too. As anticipated, Fig. 9-c shows that the total pumping power will increase massively by the increase of productivity of the system.

At the same time, the increase in the steam quality would cause a remarkable decrease in the power load on the pumps. Increasing the steam quality would cause a remarkable decrease in the power from 1800 kW down to 1000 kW saving by this a percentage of 55% of pumping power. The same behavior has been noticed on Fig. 9-d related to the NF area, m². Lower system productivity would need lower NF area. Furthermore, increasing the steam quality would decrease the needed NF area leading to cost a remarkable reduction behavior. For instance, at 40% of steam quality, the NF area has been decreased from 50 m² @ 1500m³/day down to ~25 m² @ 500m³/day. Increasing the steam quality will cause a slightly decrease in the specific power consumption as shown in Fig. 9-e.

Well depth will be in increasing mode as expected on Fig. 9-f. It would be a challenge to log into the geothermal field by a depth of 7 km for a steam quality over 40%. For normal operations, 35% of the steam quality can be used to reduce the time and tube length through the well. As expected, the temperature of the water leaving the well (see Fig. 9-g) has increased to meet the requirement of the steam. Increasing the steam quality would increase the well temperature and well depth too. A value of 30–35% is considered remarkable and quite suitable to avoid high ranges of well temperature putting in mind the NaCl effect under high temperature ranges.

The same behavior was noticed on Fig's 9-h, i. Increasing the steam quality would increase the brine blow down salinity ratio that exiting the flash tank, and the silica concentration ratio, ppm. To avoid and to reduce such effect putting in mind the cost aspects, a value of 35% would be enough for the steam quality. Fig. 10 shows the process modelling on the T-S diagram. For the 1st case, the figure shows that increasing the steam temperature (condenser) would increase the well temperature, i. e. increasing the digging costs. The figure also shows that by decreasing the steam temperature (condenser in case II) the well temperature will be decreased too, i.e decreasing the digging costs and generating more steam @ 50% quality.

4.3. The greenhouse effect results

Greenhouse gases have far-ranging environmental and health effects. They cause climate change by trapping heat and contribute to respiratory disease from smog and air pollution. Thence, it is quite important to measure the impact of the proposed system on the GHG. That impact would measure the other side of the system's reliability. Measuring the mass of the CO₂ emissions enables better carbon accounting so that emission reductions can be quantified and verified. Fig. 11 shows the production rates of the CO₂ based on different production rates (500 to 5000 m³/day). It is quite clear from the attached figure that increasing the production rate would produce more amounts of CO₂. For instance, at 500 m³/day, the total amount of tCO₂ was about 50 tCO₂ where the geothermal part has the share of 82% vs ~18% for the nanofiltration part. For 5000 m³/day, the total emissions were about 507.8 tCO₂ i.e. representing about a 90% increase if compared to the 500 m³/day. At 5000 m³/day, the emission of the geothermal part was about 417–420 tCO₂ i.e. representing a 82% of the total emissions. The nanofiltration was found representing a 18% of the total emissions.

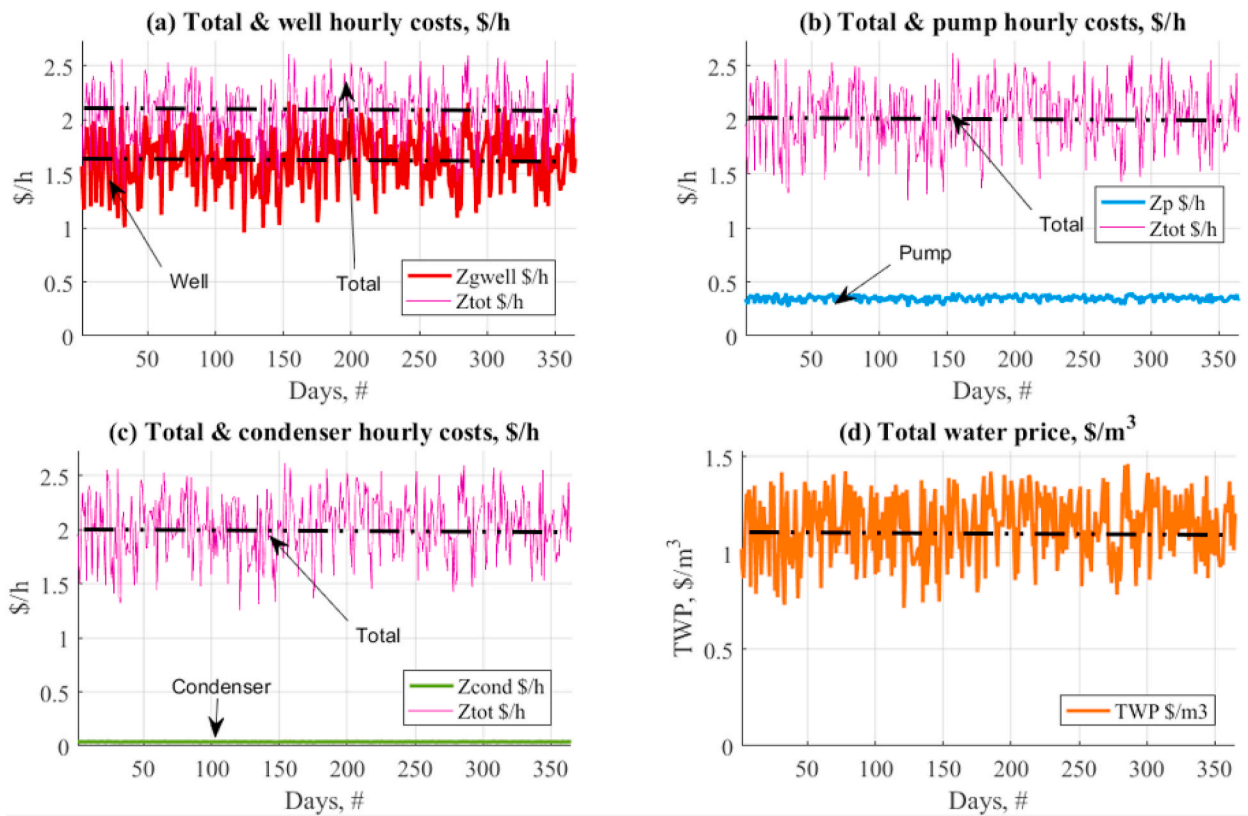


Fig. 6. Daily data results along one year related to hourly costs and total water price parameters.

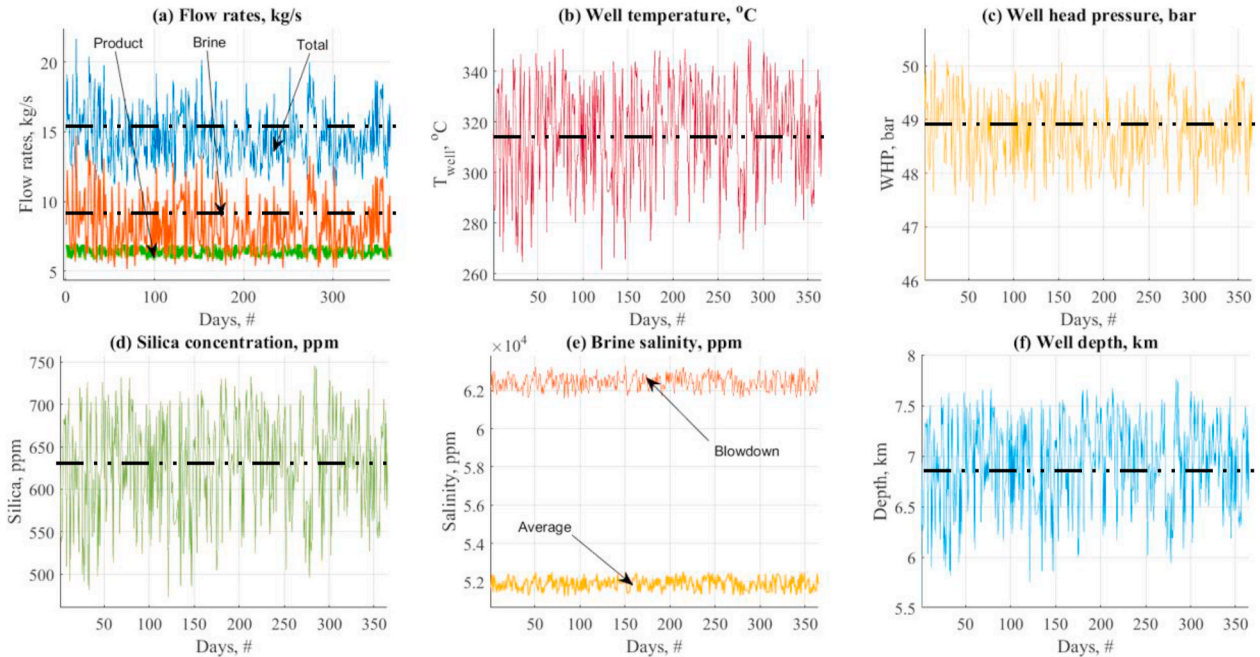


Fig. 7. Daily data results along one year related to design aspects of the proposed system.

5. Conclusion

A preliminary novel system for direct vapor generation desalination purposes has been introduced. The system's novel idea is about utilizing geothermal energy as the main source of thermal power for desalination via condensation instead of using conventional thermal techniques such

as multi-effect distillation and/or multi-stage flash. The novel idea is centralized about pumping saline or seawater into the geothermal well and use it as a brine heater unit for steam generation process. To reduce the salinity gradients through the piping system (from 45,000ppm down to 2000ppm), a Nanofiltration unit has been used as a pre-stage. Moreover, the salt rejection percentage should be varying between

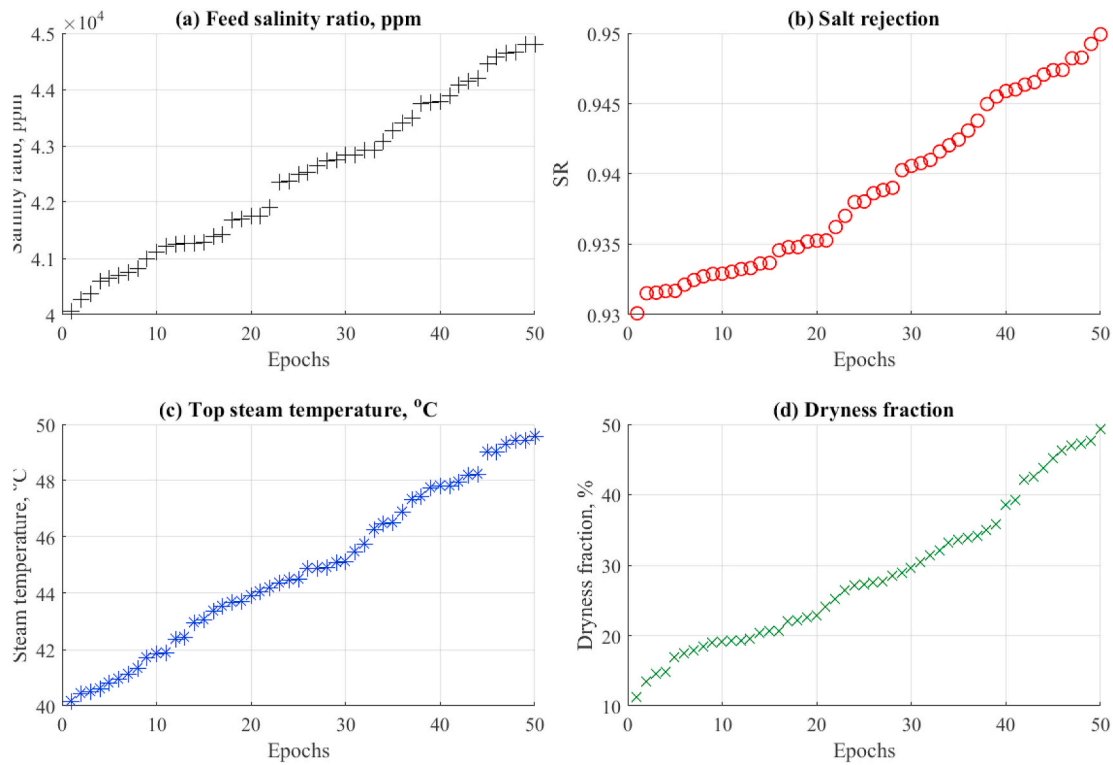


Fig. 8. Data input parameters for the proposed system.

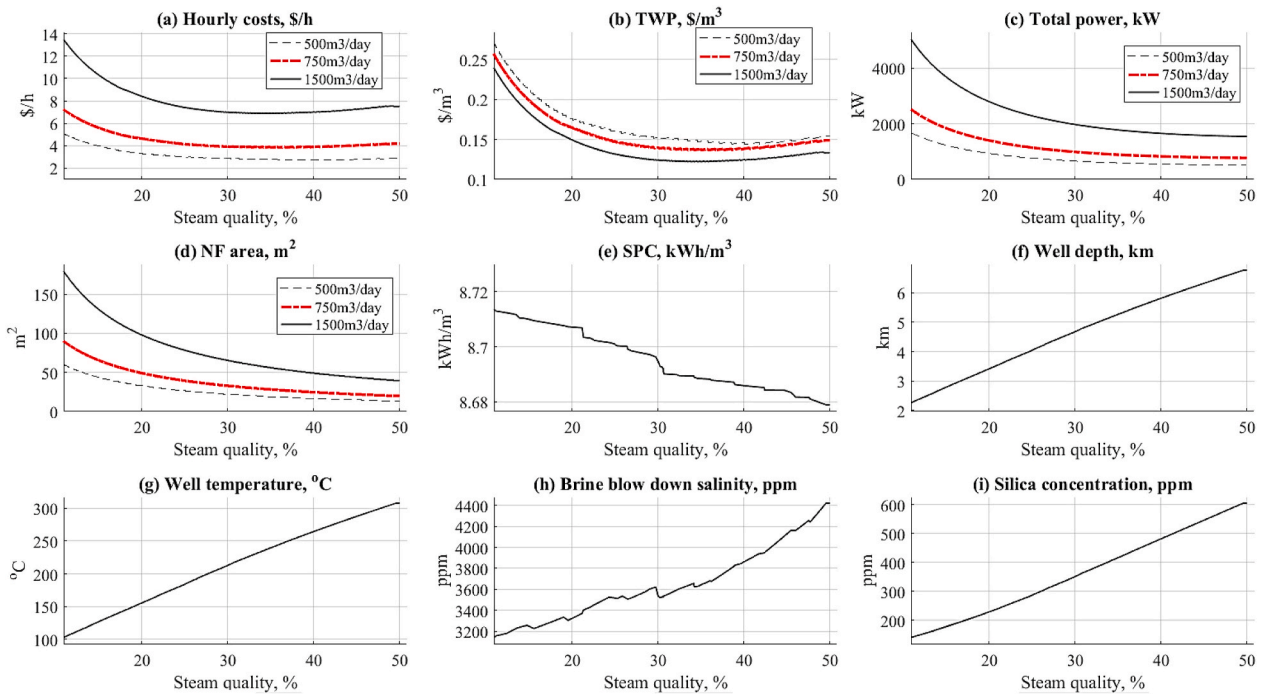


Fig. 9. Data results of the proposed system based on the data entry from Fig. 8.

0.93 and 0.95 through the Nanofiltration. Furthermore, to prevent leakage from the geothermal well, it is highly recommended to use a U-tube heat exchanger through the well. Flashing tank has been also used for the brine/steam generation. The end condenser unit is responsible for the condensation and distillate production. The system has been modeled to measure some important indicators such as total water price, hourly costs, well temperature, brine loss, well depth, and the CO₂

production rate to the environment. These mentioned indicators are performed based on controlling some important parameters such as total system productivity (500–1500m³/day), top steam temperature, and salinity ratios. Based on the analysis performed in this work, the following conclusions could be withdrawn:

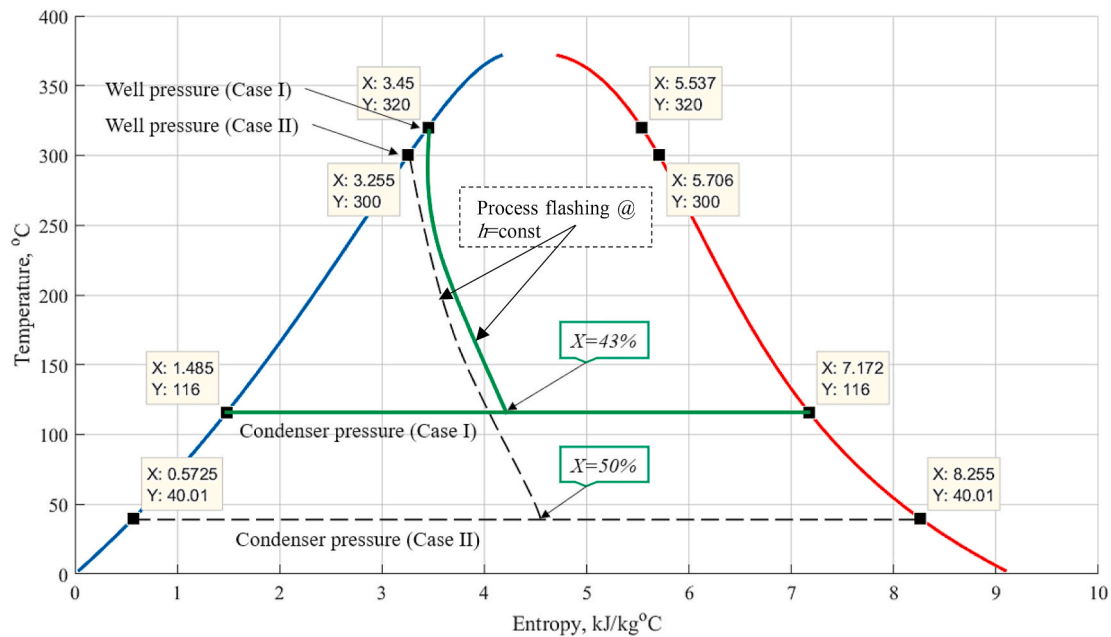


Fig. 10. The T-S diagram for the process modelling.

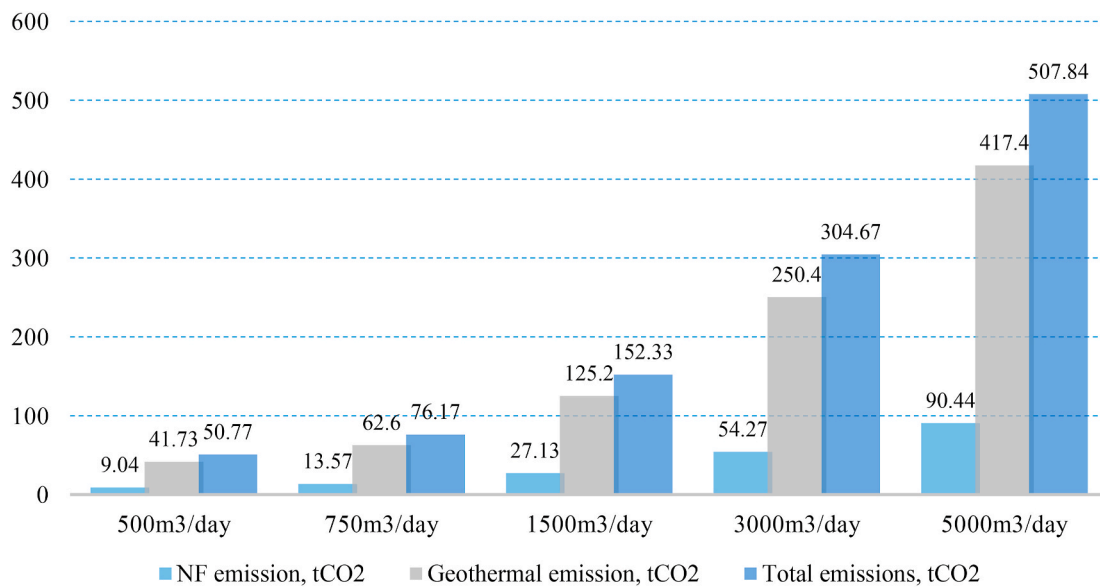


Fig. 11. The CO₂ emissions based on different levels of production rates.

- Two methodologies have been adopted where the 1st is to run the model based on salinity operating conditions. While the 2nd is to run the model based on steam quality variation and the low range of the steam temperature (40–50 °C). For the 1st case, the brine blow-down salinity (TDS) from the flash tank is assigned as input and varying between 2000ppm and 20,000ppm. For the 2nd case, the steam quality will be assigned as an input and the brine blow down will be calculated.
- The top steam temperature should not exceed over 100–120 °C in case of considering the salinity ratio technique (1st method). However, in the case of the dryness fraction technique (2nd method), the temperature of the steam should be lowered to the range of 40–50 °C.
- Well depth is found to be vary between 6–7 km with one injection well and two suction wells.
- The total hourly costs within the range of 2\$/h are considered a remarkable result while comparison against the conventional

desalination processes. The pumping hourly cost was in the range of 0.3–0.4\$/h which is considered relatively high by 20% of the total hourly costs while the condenser hourly costs present about 1.5% of total hourly costs. The range of total water price, \$/m³ was fluctuating between 0.7 and 1.2 \$/m³. Such values can compete against the conventional desalination processes in the same product category. Increasing the steam quality would decrease the TWP down to 0.15 \$/m³ however, it will increase the geothermal well temperature too.

- For 5000 m³/day, the total emissions were about 507.8 tCO₂ i.e. representing about a 90% increase if compared to the 500 m³/day.

Declaration of competing interest

The authors declare that they have no known competing financial interests or personal relationships that could have appeared to influence the work reported in this paper.

Acknowledgement

This research idea was supported and created by Abdullah Almtairi, Civil and environmental engineering, Faculty of Science & Engineering, University of Wolverhampton, England. We would also like to show our gratitude to the Wolverhampton University, Al-Jouf University, Sakaka, Saudi Arabia, and REDS Library organization for sharing their pearls of wisdom with us during this research.

Nomenclature

| | |
|------------------------|--|
| <i>A</i> | Area, m ² |
| <i>A_f</i> | Amortization factor, 1/y |
| <i>C</i> | Capacitance for heat exchanger, kJ/s ^o C |
| <i>C_p</i> | Specific heat capacity, kJ/kg ^o C @ constant pressure |
| <i>D</i> | Diameter, m |
| <i>EM</i> | Tends to emission |
| <i>EM_f</i> | Emission factor, g/kWh, t/MWh |
| <i>Geo</i> | Tends to geothermal |
| <i>HP</i> | High pressure pump, kW |
| <i>h</i> | Enthalpy, kJ/kg |
| <i>ID_{nf}</i> | Nanofiltration membrane diameter, m |
| <i>L</i> | Length, m |
| <i>LF</i> | Load factor, % |
| <i>M</i> | Mass flow rate, m ³ /h, kg/s |
| <i>M_{pt}</i> | Total productivity, kg/s or m ³ /day |
| <i>M_{pnf}</i> | Nanofiltration productivity, kg/s or m ³ /day |
| <i>n</i> | Number, # |
| <i>NF</i> | Nanofiltration |
| <i>NOP</i> | Number of passes, # |
| <i>NTU</i> | Number of transfer units, # |
| <i>OH</i> | Operating hours, h |
| <i>P</i> | Power, kW, or Pressure, bar |
| <i>ΔP</i> | Pressure, bar |
| <i>Q</i> | Thermal power, kW |
| <i>RR</i> | Recovery ratio |
| <i>S</i> | Salinity ratio, ppm |
| <i>SPC</i> | Specific power consumption, kWh/m ³ |
| <i>SR</i> | Salt rejection |
| <i>T</i> | Temperature, °C |
| <i>TWP</i> | Total Water Price, \$/m ³ |
| <i>U</i> | Overall heat transfer, W/m ^{2o} C |
| <i>V</i> | Volume, cm ³ |
| <i>W</i> | Work, kW |
| <i>X</i> | Dryness fraction |
| <i>Z</i> | Hourly costs, \$/h |

Subscripts

| | |
|--------------|--------------------|
| <i>av</i> | Average |
| <i>b</i> | Brine |
| <i>cond</i> | Condenser |
| <i>cold</i> | Cold side |
| <i>cw</i> | Cooling water |
| <i>cond</i> | Condenser |
| <i>d</i> | Distillate product |
| <i>f</i> | Feed, or factor |
| <i>gwell</i> | Geothermal well |
| <i>fsh</i> | Flash tank |
| <i>h</i> | High |
| <i>hot</i> | Hot side |
| <i>i</i> | Inlet |
| <i>loss</i> | Losses |
| <i>nf</i> | Nanofiltration |
| <i>o</i> | Out |
| <i>p</i> | Product or pump |
| <i>pipe</i> | Pipe |

| | |
|---------------|---------------------------------|
| <i>st</i> | Steam |
| <i>si</i> | Inlet steam |
| <i>so</i> | Outlet steam |
| <i>t, tot</i> | Total |
| <i>ti,o</i> | Flash tank inlet and/or outlet |
| <i>tnf</i> | Total related to nanofiltration |
| <i>w</i> | Water |
| <i>well</i> | Well |

Greek

| | |
|----------|----------------------------|
| <i>η</i> | Efficiency, % |
| <i>ρ</i> | Density, kg/m ³ |
| <i>ε</i> | Effectiveness |
| <i>μ</i> | Viscosity, Pa.s |

References

- Akin, Serhat, Orucu, Yasemin, Fridriksson, Thrainn, 2020. Characterizing the Declining CO₂ Emissions from Turkish Geothermal Power Plants, PROCEEDINGS, 45 Workshop on Geothermal Reservoir Engineering, Stanford University, Stanford, California. SGP-TR-216.
- Al-Harbi, Omar, 2011. Karl Lehnert, Al-Khafji Solar Water Desalination. The Saudi International Water Technology Conference.
- Alirahmi, Seyed Mojtaba, Rahmani Dabbagh, Sajjad, Ahmadi, Pouria, Wongwises, Somchai, 2020. Multi-objective design optimization of a multi-generation energy system based on geothermal and solar energy. Energy Convers. Manag. 205, 112426. <https://doi.org/10.1016/j.enconman.2019.112426>.
- Amin, Mohammadi, Mehrpooya, Mehdi, 2017. Energy and exergy analyses of a combined desalination and CCHP system driven by geothermal energy. Appl. Therm. Eng. 116, 685–694. <https://doi.org/10.1016/j.applthermaleng.2017.01.114>.
- arabnews. Arabnews. <https://www.arabnews.com/node/349724>.
- Boucekima, B., 2003. Solar desalination plant for small size use in remote arid areas of South Algeria for the production of drinking water. Desalination 156 (1–3), 353–354. [https://doi.org/10.1016/S0011-9164\(03\)00367-9](https://doi.org/10.1016/S0011-9164(03)00367-9). Aug 1.
- Bourouni, K., Martin, R., Tadriss, L., 1999. Analysis of heat transfer and evaporation in geothermal desalination units. Jul 7 Desalination (2), 122. [https://doi.org/10.1016/S0011-9164\(99\)00050-8](https://doi.org/10.1016/S0011-9164(99)00050-8), 301–13.
- Burkhardt, J.J., Heath, G., Cohen, E., 2012. Life cycle greenhouse gas emissions of trough and tower concentrating solar power electricity generation. J. Ind. Ecol. 16, S93–S109. <https://doi.org/10.1111/j.1530-9290.2012.00474.x>.
- Calise, Francesco, Vanoli, Laura, Massimo, Dentice d'Accadia, Macaluso, Adriano, Piacentino, Antonio, 2016. A novel solar-geothermal trigeneration system integrating water desalination: design, dynamic simulation and economic assessment. Energy 115, 1533–1547. <https://doi.org/10.1016/j.energy.2016.07.103>.
- Cornejo, P.K., Santana, M.V.E., Hokanson, D.R., Mihelcic, J.R., Zhang, Q., 2014. Carbon footprint of water reuse and desalination: a review of greenhouse gas emissions and estimation tools. J. Water Reuse Desalination 4, 238–252. <https://doi.org/10.2166/wrd.2014.058>.
- Darwish, M.A., Abdulrahim, H.K., Hassan, A.S., Mabrouk, A.A., 2015. PV and CSP solar technologies & desalination: economic analysis. Desalination Water Treat. 1–23. <https://doi.org/10.1080/19443994.2015.1084533>.
- DiPippo, Ronald, 2007. Geothermal Power Plants: Principles, Applications, Case Studies, and Environmental Impacts, second ed., ISBN 9780750686204.
- El-Dessouky, Hisham T., Ettouney, Hisham M., 2002. Fundamental of Saltwater Desalination. Kuwait University, Elsevier Science (book).
- El-Nashar, Ali M., 2001. The economic feasibility of small solar MED seawater desalination plants for remote arid areas. Desalination 134, 173–186. [https://doi.org/10.1016/S0011-9164\(01\)00124-2](https://doi.org/10.1016/S0011-9164(01)00124-2).
- Fath, H., 2000. Desalination Technology: the Role of Egypt in the Region. 5th International Water Technology Conference, Alexandria, Egypt.
- Gharibi, Shabnam, Mortezaazadeh, Emad, Seyed Jalaledin Hashemi Aghcheh Badi, Ali, Vatani, 2018. Feasibility study of geothermal heat extraction from abandoned oil wells using a Utube heat exchanger. Energy. <https://doi.org/10.1016/j.energy.2018.04.003>.
- Gupta, Harsh, Roy, Sukanta, Geothermal Energy, 2007. An Alternative Resource for the 21st Century. Elsevier, p. 978 (book), 0-444-52875-9.
- Iaquaniello, G., Salladini, A., Mabrouk, A.A., Fath, H.E.S., 2014. Concentrating solar power (CSP) system integrated with MED-RO hybrid desalination. Desalination 336, 121–128. <https://doi.org/10.1016/j.desal.2013.12.030>.
- Incropera, Frank P., DeWitt, David P., 2002. Fundamentals of Heat and Mass Transfer. J. Wiley, New York (book).
- Jia, X., Klemeš, J.J., Varbanov, P.S., Wan Alwi, S.R., 2019. Analyzing the energy consumption, GHG emission, and cost of seawater desalination in China. Energies 12, 463. <https://doi.org/10.3390/en12030463>.
- Karytsas, C., Mendrinou, D., Goldbrunner, J., 2003. Low enthalpy geothermal energy utilisation schemes for greenhouse and district heating at Traianoupolis Evros, Greece. Geothermics 32 (1), 69–78. [https://doi.org/10.1016/S0375-6505\(02\)00051-2](https://doi.org/10.1016/S0375-6505(02)00051-2).
- Kolahi, Mohammad-Reza, Amidpour, Majid, Yari, Mortaza, 2020. Multi-objective metaheuristic optimization of combined flash-binary geothermal and humidification

- dehumidification desalination systems. *Desalination* 490. <https://doi.org/10.1016/j.desal.2020.114456>, 114456.
- Lee, C.K., Lam, H.N., 2008. Computer simulation of borehole ground heat exchangers for geothermal heat pump systems. *Renew. Energy* 33 (6), 1286–1296. <https://doi.org/10.1016/j.renene.2007.07.006>.
- Loutatidou, Savvina, Hassan, A., 2015. Arafat, Techno-economic analysis of MED and RO desalination powered by low-enthalpy geothermal energy. *Desalination* 365, 277–292. <https://doi.org/10.1016/j.desal.2015.03.010>.
- Mabrouk, Abdel Nasser, Fath, Hassan S., 2013. Experimental study of high-performance hybrid NF-MSF desalination pilot test unit driven by renewable energy. *Desalination Water Treat.* 6895–6904. <https://doi.org/10.1080/19443994.2013.773860>.
- Mabrouk, A.A., Nafey, A.S., Fath, H.E.S., 2007. Thermoeconomic analysis of some existing desalination processes. *Desalination* 205, 354–373. <https://doi.org/10.1016/j.desal.2006.02.059>.
- Mabrouk, Abdel Nasser, Koc, Muammer, Ahmed, Abdala, 2017. Technoeconomic analysis of tri- hybrid reverse osmosis-forward osmosis- multi-stage flash desalination process. *Desalination Water Treat.* 98, 1–15. <https://doi.org/10.5004/dwt.2017.21564>.
- Mahmoudi, H., Spahis, N., Goosen, M.F., Ghaffour, N., Drouiche, N., Ouagued, A., 2010. Application of geothermal energy for heating and fresh water production in a brackish water greenhouse desalination unit: a case study from Algeria. *Renew. Sustain. Energy Rev.* 14 (1), 512–517. <https://doi.org/10.1016/j.rser.2009.07.038>.
- Manenti, Flavio, Masi, Maurizio, Santucci, Giorgio, Manenti, Giovanni, 2013. Parametric simulation and economic assessment of a heat integrated geothermal desalination plant. *Desalination* 317, 193–205. <https://doi.org/10.1016/j.desal.2013.02.027>.
- Nafey, A.S., Sharaf, M.A., 2010. Lourdes García-Rodríguez, A new visual library for design and simulation of solar desalination systems (SDS). *Desalination* 259, 197–207. <https://doi.org/10.1016/j.desal.2010.04.005>.
- Nafey, A.S., Fath, H.E.S., Mabrouk, A.A., 2006. A new visual package for Design and simulation of desalination processes. *Desalination* 194, 281–296. <https://doi.org/10.1016/j.desal.2005.09.032>.
- Nafey, A.S., Fath, H.E.S., Mabrouk, A.A., 2006a. Thermoeconomic investigation of multi effect evaporation (MEE) and hybrid multi effect evaporation-multi stage flash (MEE-MSF) systems. *Desalination* 201, 241–254. <https://doi.org/10.1016/j.desal.2005.09.044>.
- Noorollahi, Younes, Taghipoor, Salman, Sajadi, Behrang, 2017. Geothermal sea water desalination oil/gas system (GSWDS) using abandoned wells. *Geothermics* 67, 66–75. <https://doi.org/10.1016/j.geothermics.2017.01.008>.
- Nordin, A., Amin, M., Majid, A., 2013. Analysis of carbon dioxide emission of gas fuelled cogeneration plant. *IOP Conf. Ser. Mater. Sci. Eng.* 50 <https://doi.org/10.1088/1757-899X/50/1/012054>, 012054.
- Østergaard, P.A., Lund, Henrik, 2011. A renewable energy system in Frederikshavn using low-temperature geothermal energy for district heating. *Appl. Energy* 88 (2), 479–487. <https://doi.org/10.1016/j.apenergy.2010.03.018>.
- Oulhazzan, M., Nachtane, M., Aroussy, Y., Saifaoui, D., Winninger, D., Rouway, M., 2016. Linear Fresnel Concentrator with dual energy solar tracking Application: seawater desalination. *European Journal of Scientific Research*. <http://www.europeanjournalofscientificresearch.com>.
- Rees, S.J., 2015. An extended two-dimensional borehole heat exchanger model for simulation of short and medium timescale thermal response. *Renew. Energy* 83 (Suppl. C), 518–526. <https://doi.org/10.1016/j.renene.2015.05.004>.
- Rodríguez, G., Rodríguez, M., Perez, J., Veza, J., 1996. A systematic approach to desalination powered by solar, wind and geothermal energy sources. In: *Proceedings of the Mediterranean Conference on Renewable Energy Sources for Water Production*. European Commission, EUORED Network, CRES, p. 20. , EDS, 10-12 June 1996, Santorini.
- Rosiek, S., Battles, F.J., 2012. Shallow geothermal energy applied to a solar-assisted air-conditioning system in southern Spain: two-year experience. *Appl. Energy* 100, 267–276. <https://doi.org/10.1016/j.apenergy.2012.05.041>.
- Sahana, Chitta, De, Sudipta, Mondal, Subha, 2021. Integration of CO2 power and refrigeration cycles with a desalination unit to recover geothermal heat in an oilfield. *Appl. Therm. Eng.* 189 <https://doi.org/10.1016/j.applthermaleng.2021.116744>, 116744.
- Salehi, S., Mahmoudi, S. Mohammad S., Yari, M., Rosen, M.A., 2018. Multi-objective optimization of two double-flash geothermal power plants integrated with absorption heat transformation and water desalination. *J. Clean. Prod.* 195, 796–809. <https://doi.org/10.1016/j.jclepro.2018.05.234>.
- Sarbaty, Rosalam, Chiam, Chel-Ken, 2013. Evaluation of geothermal energy in desalination by vacuum membrane distillation. *Appl. Energy* 112, 737–746. <https://doi.org/10.1016/j.apenergy.2012.12.028>.
- Sharaf Eldean, Mohamed A., Soliman, A.M., 2013. A New Visual Library for Modeling and Simulation of Renewable Energy Desalination Systems (REDS), *Desalination and Water Treatment*. <https://doi.org/10.1080/19443994.2013.777369>.
- Sharaf Eldean, M.A., Thesis, PhD., 2011. *Design and Simulation of Solar Desalination Systems* (Philography No. 11114571).
- Soliman, A.M., Al-Falahi, Adil, Sharaf Eldean, Mohamed A., Elmnifi, Monaem, Hassan, Magdi, Younis, Basim, Mabrouk, Abdelnasser, Hassan, E., Fath, S., 2020. A new system design of using solar dish-hydro combined with reverse osmosis for sewage water treatment: case study Al-Marj, Libya. *Desalination Water Treat.* 193, 189–211. <https://doi.org/10.5004/dwt.2020.25782>.
- Tomaszewska, Barbara, 2013. Michał Bodzek, Desalination of geothermal waters using a hybrid UF-RO process. Part I: boron removal in pilot-scale tests. *Desalination* 319, 99–106. <https://doi.org/10.1016/j.desal.2012.05.029>.
- Walid, A., 2007. Abderrahman, water management in ArRiyadh. *Int. J. Water Resour. Dev.* 22, 277–289. <https://doi.org/10.1080/07900620600654785>.